Topographic Controls On the Development of Contemporaneous but Contrasting Basin-Floor Depositional Architectures

DOI:
10.2110/jsr.2018.58

Document Version
Accepted author manuscript

Running head: TOPOGRAPHIC CONTROLS ON BASIN-FLOOR DEPOSITIONAL ARCHITECTURE

Title: TOPOGRAPHIC CONTROLS ON THE DEVELOPMENT OF CONTEMPORANEOUS BUT CONTRASTING BASIN-FLOOR DEPOSITIONAL ARCHITECTURES

Authors: DANIEL BELL[1], CHRISTOPHER J. STEVENSON[2], IAN A. KANE[1], DAVID M. HODGSON[3], MIQUEL POYATOS-MORÉ[4]

Institutions:

[1] SedRESQ, School of Earth and Environmental Sciences, University of Manchester, Manchester, M13 9PL, U.K.

[2] School of Environmental Sciences, University of Liverpool, Liverpool, L69 3GP, U.K.

[3] The Stratigraphy Group, School of Earth and Environment, University of Leeds, Leeds, LS2 9JT, U.K.

[4] Department of Geosciences, University of Oslo, 0371 Oslo, Norway

Email: daniel.bell-2@manchester.ac.uk

Keywords: Structurally confined basin, deep-water fan, hybrid event beds, lobe stacking, flow deflection

ABSTRACT

Sediment-laden gravity-driven flow deposits on the basin-floor are typically considered to form either discrete lobes that stack compensationally, or packages of laterally extensive beds, commonly termed ‘sheets’. These end-member stacking patterns are documented in several basin-fills. However, whether they can co-exist in a single basin, or there are intermediate or transitional stacking patterns is poorly understood. An analysis of depositional architecture and stacking patterns along a 70 km dip-orientated transect within the Upper Broto Turbidite System (Jaca Basin, south-central Pyrenees, Spain), which displays disparate stacking patterns within contemporaneous strata, is presented. Proximal and medial deposits are characterized by discrete packages of clean sandstones with sharp bed-tops which exhibit predictable lateral and longitudinal facies changes, and are interpreted as lobes. Distal deposits comprise both relatively clean sandstones and hybrid beds that do not stack to form lobes. Instead, localized relatively-thick hybrid beds are inferred to have inhibited the development of lobes. Hybrid beds developed under flows which were deflected and entrained carbonate mud substrate off a carbonate slope that bounded the basin to the south; evidence for this interpretation includes: 1) divergent paleoflow indicators and hummock-like features in individual beds; 2) a decrease in hybrid bed thickness and abundance away from the lateral confining slope; 3) a carbonate-rich upper-division, not seen in more proximal turbidites. The study demonstrates the co-occurrence of different styles of basin-floor stacking patterns within the same stratigraphic interval, and suggests that that characterization of deep-water systems as either lobes or sheets is a false dichotomy.

INTRODUCTION

Submarine fans represent some of the largest sedimentary deposits on Earth (e.g. Barnes and Normark, 1985), can contain significant volumes of hydrocarbons (e.g. McKie et al., 2015), and are the ultimate sink for vast quantities of organic carbon (e.g. Cartapanis et al., 2016) and pollutants (e.g. Gwiazda et al., 2015). Despite their economic and environmental importance, the processes and products of submarine fans are relatively poorly-understood, due to limitations associated with remote sensing and monitoring of modern systems, and challenges with imaging and sampling buried ancient systems. Consequently, uplifted ancient fans at outcrop represent an opportunity to study the architecture of these systems at a high resolution (e.g. Walker, 1966; Ricci-Lucchi and Valmori, 1980; Mutti and Sonnino, 1981; Hodgson et al., 2006; Grundvåg et al., 2014).

Sediment-laden gravity-driven flows develop deposits which are typically considered to stack in one of two end-member patterns on the basin-floor: i) compensational lobes; or ii) individual laterally extensive beds, commonly termed ‘sheets’ (referred to as tabular stacking herein; e.g. Ricci-Lucchi and Valmori, 1980; Mutti and Sonnino, 1981; Talling et al., 2007; Deptuck et al., 2008; Prélat et al., 2009; Marini et al., 2015; Fonnesu et al., 2018). Basin-floor lobes form discrete composite sand-bodies with subtle convex-upward topography and display predictable bed thickness and facies changes (e.g. Prélat et al., 2009; Grundvåg et al., 2014; Marini et al., 2015; Spychala et al., 2017a). Compensational stacking occurs where depositional relief causes subsequent flows to be routed to and deposited in adjacent topographic lows, as documented from outcrop (Mutti and Sonnino, 1981; Prélat et al., 2009; Prélat and Hodgson, 2013; Grundvåg et al., 2014; Marini et al., 2015); seismic and seabed imaging (Deptuck et al., 2008; Jegou et al., 2008; Saller et al., 2008; Straub et al., 2009; Picot et al., 2016); and experimental studies (Parsons et al., 2002). Tabular stacking has been described in basin settings where flows were fully contained, or laterally confined (e.g. Hesse, 1964; Ricci-Lucchi and Valmori, 1980; Ricci-Lucchi, 1984; Remacha and Fernández, 2003; Tinterri et al., 2003; Amy et al., 2007; Marini et al., 2015). Tabular beds can be traced over tens to hundreds of kilometers and can be basin-wide (e.g. Hirayama and Nakajima, 1977; Ricci-Lucchi and Valmori, 1980; Talling et al., 2007; Stevenson et al., 2014a). Deep-water depositional systems are usually considered to exhibit one style of stacking pattern or the other. However, recent studies recognize that different stacking patterns can develop at different stratigraphic levels within the same basin-fill (Marini et al., 2015; Fonnesu et al., 2018). Here, we present a detailed study of two contrasting types of stacking pattern co-occurring within the same well-constrained stratigraphic interval of a confined basin for the first time.

Confined basins are characterized by intrabasinal slopes and may include syn-sedimentary structural features, which can influence flow behaviour, and therefore depositional processes and patterns (e.g. Haughton, 1994; Kneller and McCaffrey, 1995; Kneller and McCaffrey, 1999; Hodgson and Haughton, 2004; Remacha et al., 2005; Amy et al., 2007; Pickering and Bayliss, 2009; Kane et al., 2010; Muzzi Magalhaes and Tinterri, 2010; Tinterri et al., 2017). Hybrid beds are a common component of unconfined deep-water systems, and are predominantly identified in fringe locations (e.g. Haughton et al., 2003; Talling et al., 2004; Haughton et al., 2009; Hodgson, 2009; Kane and Pontén, 2012; Grundvåg et al., 2014; Kane et al., 2017; Spychala et al., 2017a; Spychala et al., 2017b; Fonnesu et al., 2018). However, recent work suggests hybrid beds also form where flows interact with, and decelerate against, confining slopes (e.g. McCaffrey and Kneller, 2001; Muzzi Magalhaes and Tinterri, 2010; Patacci and Haughton, 2014; Fonnesu et al., 2015; Southern et al., 2015; Tinterri and Tagliaferri, 2015). These models generally do not incorporate the effects of slope substrate entrainment during flow deflection and transformation (although see 'sandwich beds' of McCaffrey and Kneller, 2001), the deposits of which are discussed as an important process in generating basin-floor topography in distal settings.

This study examines stacking patterns and facies distributions of time-equivalent deep-water stratigraphy deposited within a confined, tectonically-active basin: the Upper Broto Turbidite System of the Jaca Basin, northern Spain. The following research questions are addressed: 1) how are turbidites and other gravity flow deposits distributed spatially within a basin that variably confined the parent flows spatially? 2) What is the spatial distribution of stacking patterns? 3) Where are hybrid beds developed and how do they affect the facies distributions and stacking of basin floor deposits? 4) What controlled the development of hybrid beds?

GEOLOGICAL SETTING

The Jaca Basin (Fig. 1), located in the south-central Pyrenees, developed during the Early Eocene as an elongate east-west trending foredeep approximately 175 km long and 40-50 km wide (Puigdefàbregas et al., 1975; Mutti, 1984; Labaume et al., 1985; Mutti, 1985; Mutti, 1992; Teixell and García-Sansegundo, 1995; Remacha and Fernández, 2003; Fernández et al., 2004; Millán-Garrido et al., 2006). The basin was bounded by the Pyrenean orogenic belt to the north, a carbonate-dominated ramp-type margin to the south, and the Boltaña Anticline and the Aínsa Basin to the east (Figs. 1C, 2; Puigdefàbregas et al., 1975; Labaume et al., 1985; Barnolas and Teixell, 1994). Fluvial-to-shallow marine systems of the Tremp-Graus Basin, located to the east, fed clastic sediment into the Aínsa and Jaca Basins through structurally-confined channels and canyons (Fig. 1C; e.g. Nijman and Nio, 1975; Mutti, 1984; Mutti et al., 1988; Mutti, 1992; Payros et al., 1999; Moody et al., 2012; Bayliss and Pickering, 2015). The fill of the Aínsa Basin is interpreted as a submarine slope succession (e.g. Mutti, 1977; Millington and Clark, 1995; Clark and Pickering, 1996; Pickering and Corregidor, 2005; Pickering and Bayliss, 2009; Moody et al., 2012), which delivered sediment to the basin-floor environments of the Jaca Basin (Figs. 1C, 2; Mutti, 1977; Mutti 1984; Mutti, 1985; Remacha and Fernández, 2003; Remacha et al., 2005).

The Hecho Group in the Jaca Basin comprises submarine-lobe and basin-plain deposits with paleocurrents predominantly to the northwest (Mutti, 1977; Mutti, 1992; Remacha et al., 2005; Clark et al., 2017). The deep-water stratigraphy in the Jaca Basin is constrained through nine carbonate-rich megabeds (named MT-1 to -9 to maintain consistency with nomenclature), which extend 10s – 100s km from southeast to northwest (Fig. 1B; e.g. Rupke, 1976; Seguret et al., 1984; Labaume et al., 1985;

Labaume et al., 1987; Rosell and Wiezorek, 1989; Barnolas and Teixell, 1994; Payros et al., 1999). Locally, these deposits can be over 100 m thick and contain rafted blocks 10s m thick and 100s m wide. These distinctive beds can be mapped regionally and enable correlation between isolated outcrops (e.g. Remacha and Fernández, 2003).

Previous studies in the Jaca Basin have described both tabular stacking patterns (Remacha and Fernández, 2003; Tinterri et al., 2003; Remacha et al., 2005), and compensationally stacked lobes developed due to autogenic avulsion of feeder channels, or through structural controls (Mutti, 1992; Clark et al., 2017). Across-strike architecture is poorly constrained due to a relatively narrow outcrop belt trending approximately along depositional dip (Fig. 1B; e.g. Remacha and Fernández, 2003; Tinterri et al., 2003; Remacha et al., 2005). This study examines the strata of the Upper Broto turbidite system immediately underlying Megabed 4 (Fig. 2; MT-4).

DATASET AND METHODS

The field area is located along a SE – NW transect between the villages of Fanlo and Ansó (Fig. 3). Exposures along road cuts, small gullies and river valleys permit detailed study of stratigraphic sections and the ability to trace bed geometries over 100s meters. Sixteen sedimentary logs were collected over a 70 km depositional dip and 1.5 km depositional strike transect. Sections were logged at centimeter-scale, including individual bed thicknesses and sedimentary textures. Sandstone packages were correlated using three marker beds in order to produce a robust correlation framework. These beds, in stratigraphic order, are: Db-1 (debrite-1), Db-2 and MT-4. MT-4 is mappable across the study area (e.g. Payros et al., 1999), Db-1 and Db-2 are locally present in the study area around Broto (Fig. 3). MT-4 has previously been used as a marker bed by Remacha and Fernández (2003), to constrain the same studied interval in distal localities. Paleocurrent readings (n = 166) were collected from flute and groove casts, and 3D ripple cross-lamination. Lithofacies are described and interpreted in Table 1.

FACIES ASSOCIATIONS

Correlation of bed packages, both down depositional-dip and across-strike, shows that they thicken and thin over 100s to 1000s m, passing from thick-bedded sandstones into fine-grained, thin-bedded heterolithic intervals. They have lobate geometries similar to those reported from basins where lobes are identified (Prélat et al., 2009; Grundvåg et al., 2014; Marini et al., 2015). Beds within lobes exhibit broadly tabular geometries on a 10s to 100s m scale where observed in outcrop, with localized decimeter- to meter-scale scouring. Between lobes, fine-grained and thin-bedded packages can be traced laterally over 100s to 1000s m between outcrops. These packages are interpreted as either the distal lobe fringes of adjacent lobes, or as interlobe intervals related to reduced sediment supply to the basin (e.g. Prélat et al., 2009).

Thick-bedded sandstones

Description.--- Thick-bedded sandstone facies form 1–5 m-thick amalgamated packages comprising thick-bedded (>0.3 m-thick) structureless sandstones (Fig. 4D), and less-common planar-laminated sandstones (Fig. 4B, C). They are fine- to medium-grained and can be normally-graded or ungraded. Mudstone clasts are frequently observed along amalgamation surfaces and near bed-bases (Fig. 4C). Millimeter-scale lamination, and centimeter- to decimeter-scale low-angle cross-lamination is observed at southeastern localities (Fig. 4B).

Interpretation.--- Structureless turbidite beds, and those with millimeter-scale lamination, are interpreted to represent deposition from high-concentration turbidity currents with relatively high rates of aggradation, preventing the development of tractional sedimentary structures (e.g. Kneller and Branney, 1995; Sumner et al., 2008; Talling et al., 2012). Common amalgamation, and entrainment of mudstone-clasts within thick-bedded sandstones indicates that the parent flows were highly energetic, and capable of eroding and entraining, and bypassing sediment during the passage of the flow (e.g. Lowe, 1982; Mutti, 1992; Kneller and Branney, 1995; Gladstone et al., 2002; Talling et al., 2012; Stevenson et al., 2014b; Stevenson et al., 2015). Thick-bedded sandstone-prone packages are therefore interpreted to represent lobe axis environments (Walker, 1978; Gardner et al., 2003; Prélat et al., 2009; Grundvåg et al., 2014; Marini et al., 2015; Kane et al., 2017).

Medium-bedded sandstones

Description.--- Infrequently amalgamated 0.1 – 0.3 m thick fine- to very fine-grained sandstones which typically have sharp to weakly-erosive bed bases. Planar lamination is common, particularly in the upper half of the beds (Fig. 4C), whereas structureless sandstones are infrequently observed. Ripple cross-lamination and wavy-topped beds are common where normal grading at bed tops is present. Bed tops are usually sharp, but locally grade into fine-siltstone.

Interpretation.--- Structured sandstones represent deposition and reworking by low-concentration turbidity currents, whilst structureless sandstones represent deposition from high-concentration turbidity currents. The mixture and preservation of both high- and low-concentration turbidity current deposits suggests a less-axial location of deposition compared to thick-bedded sandstones. Amalgamated structured sandstones with planar-lamination and ripple cross-lamination have been interpreted to be associated with off-axis lobe environments, deposited by decelerating turbidity currents (Prélat et al., 2009; Marini et al., 2015; Spychala et al., 2017c). Therefore, medium-bedded sandstone-prone packages are interpreted to represent lobe off-axis environments.

Thin-bedded sandstones

Description.--- Thin-bedded, fine- to very fine-grained sandstone beds (<10 cm thick) are normally-graded and occur interbedded with fine siltstones. Ripple cross-lamination and wavy-laminated bed tops are dominant, whereas planar lamination is less common (Fig. 4A). Typically, beds have a sharp decrease in grain-size from a lower sandstone to overlying silt-rich mudstone. Packages of thin-bedded sandstones are identified on a centimeter- to decimeter-scale within thicker-bedded packages, but are also identified as meter- to decameter-scale packages between thicker-bedded packages.

Interpretation.--- Thin-bedded, structured sandstones are interpreted to be deposited from low-concentration turbidity currents (Mutti, 1992; Jobe et al., 2012; Talling et al., 2012). Wavy bedforms are interpreted to form due to later flows filling the topography of previous ripple deposits (e.g. Jobe et al., 2012). The observations are consistent with facies of lobe-fringe settings (e.g. Mutti, 1977; Prélat et al., 2009; Marini et al., 2015; Spychala et al., 2017b), and similar to the facies near Linás de Broto and Yésero (Fig. 3B) described and interpreted in the same way (Mutti, 1977).

Hybrid beds

Description.--- Hybrid beds (Fig. 5) are 0.1-3.2 m thick and are described within an idealized vertical facies scheme consisting of six divisions. Division 1 (D1) Basal, relatively clean sandstone or coarse-grained siltstone that is typically structureless, with rare planar-laminae; D2) A sharp contact to a rippled and/or wavy sandstone, which is typically clean, but is locally argillaceous; D3) A poorly-sorted, matrix-supported argillaceous sandstone (see Table 1); D4) A poorly-sorted mudstone division (see Table 1). The contact to the underlying argillaceous sandstone can be abrupt or graded (Fig. 5); D5) A gradational or abrupt contact to a silt-rich mudstone division, which can be up to 1.5 m thick; D6) A sharp to gradational contact to a white, normally graded carbonate-rich siltstone to claystone (see Table 1). The above represents an idealized sequence, and in an individual bed one or more of D2 – 6 may be absent.

Interpretation.--- Hybrid beds have been interpreted as the deposits of flows transitional between turbulent and cohesive rheologies (e.g. Haughton et al., 2003; Talling et al., 2004; Haughton et al., 2009; Hodgson, 2009; Baas et al., 2011; Kane and Pontén, 2012; Kane et al., 2017; Southern et al., 2017; Pierce et al., 2018). The vertical assemblage of facies within hybrid beds here indicates temporal flow evolution from 1) high- or low-concentration turbulent; to 2) transitional/laminar; to 3) low-concentration turbulent flow regimes. Structureless and planar-laminated sandstones in D1 are interpreted to have been deposited by high- to low-concentration turbidity currents (Table 1). The ripple cross-laminated D2 indicates a flow with a turbulent component able to tractionally rework the bed. The sharp contact between D1 and D2 suggests there was a hiatus in deposition. D3 and D4 were deposited by cohesive flows, representing the longitudinal transformation of the flow from turbulent to cohesive. D5 and D6 were likely deposited by a dilute turbidity current (e.g. Remacha et al., 2005), or as a result of suspension settling (Mutti, 1977; Remacha et al., 2005). The common grading of D4 into D5 suggests the flow became more dilute at a fixed locality through time.

Beds with repeated, poorly-sorted, deformed, clast-rich layers have also been attributed to cyclical bores within deflected flows depositing alternate relatively clean and muddier liquefied sand (Pickering and Hiscott, 1985; Remacha and Fernández, 2003; Remacha et al., 2005; Muzzi Magalhaes and Tinterri, 2010; Tinterri and Muzzi Magalhaes, 2011). In these process models, clean sandstones are attributed to weaker bores whereas liquefied sandstones are attributed to stronger bores. Massive divisions which are relatively clast-poor (e.g. D3), or with plastically deformed clasts are interpreted to form through cyclical wave loading and shearing caused by trains of strong internal waves (Remacha et al., 2005; Muzzi Magalhaes and Tinterri, 2010).

Deflected flow facies

Description.--- Hummock-type bedforms are identified in distal localities, and exhibit convex-up low-angle laminations. However, thickening and thinning of laminae observed in Hummocky Cross-stratification (Harms et al., 1975) are not clearly observed here (Fig. 6C). Hummock-type bedforms can form a large proportion of an individual bed's thickness (Fig. 6A, 6C), or can occur as a discrete upper division of a bed. Typically, beds with hummock-type bedforms comprise a lower, structureless division overlain by an upper, structured division and exhibit lenticular geometries, with amplitudes of 2 – 15 cm. Hummock-type bedforms have larger wavelengths (decimeter- to meter-scale) and amplitudes (up to 15 cm) than wavy bed tops, typically by up to an order of magnitude (Table 1).

Centimeter-scale convolute lamination (Fig. 6B) is rarely observed in proximal and medial localities (e.g. Fanlo 1), but is more common in distal localities where it is associated with hummock-type bedforms (e.g. Hecho N).

Interpretation.--- Hummock-type bedforms have been identified in confined basins, and are interpreted to form as a result of flow deflection and reflection from a confining margin (Pickering and Hiscott, 1985; Remacha et al., 2005; Tinterri, 2011; Tinterri et al., 2017). Convolute lamination can form as a result of loading (Allen, 1982), or from shear stresses imparted on unconsolidated sediment by a later flow (Allen, 1982; McClelland et al., 2011; Tinterri et al., 2016). Development of both hummock-type bedforms and convolute laminations suggests the bedforms developed through flow reworking of an unconsolidated bed, commonly observed in confined basins (e.g. Pickering and Hiscott, 1985; Tinterri et al., 2016), as opposed to loading.

Draped scour surfaces and coarse-grained lag deposits

Description.--- Scour surfaces observed in the field area range from decimeter- to meter-scale in depth and width (Fig. 4F). Scours are recognized in the southeast of the field area around Broto (Fig. 3), and decrease in scale and frequency to the northwest. The nature of the scour-fills is variable, including mudstone (Fig. 4F), poorly-sorted mudstone to coarse-grained sandstone, and thin-beds. Commonly, scour surfaces are mantled with coarse-grained lags (Fig. 4E), particularly in thick-bedded packages. Locally, coarse-grained lags are identified as an abrupt grain-size increase near bed-tops. Coarse-grained lag deposits are identified predominantly in the southeast of the field area around Sarvisé and Broto (Figs. 3, 4E).

Interpretation.--- Coarse-grained lag deposits and draped scour surfaces are interpreted as indicators of sediment bypass (e.g. Mutti and Normark, 1987; Mutti, 1992; Elliott, 2000; Gardner et al., 2003; Beaubouef, 2004; Kane et al., 2010; Stevenson et al., 2015). The presence of numerous lags and draped scour surfaces in the southeast suggests significant amounts of sediment transport and bypass through the proximal field area, to more distal localities in the northwest.

Thick chaotic units

Debrites

Description.--- Two 0.3 – 25 m thick, poorly-sorted units are identified in the southeast of the field area (Figs. 7, 8). The units consist of a poorly-sorted sheared matrix consisting of: clay-, silt- and sand-grade material; *Nummulites* shells; sandstone 'balls' (10s cm in diameter) (Fig. 7); and rafts of turbidite beds 1 – 10s m thick (Figs. 7, 8). Local entrainment of substrate into the units is observed (Fig. 7). The upper surface of these chaotic units locally undulates, with overlying beds onlapping on a decimeter- to meter-scale. In other locations, units have a comparatively flat top with relatively tabular sandstones overlying them.

Interpretation.--- Event beds with a mud-rich, poorly-sorted, sheared matrix coupled with scattered clasts of varying sizes are characteristic of 'en masse' emplacement by a debris flow; these beds are termed debris flow deposits, or debrites (e.g. Nardin et al., 1979; Iverson, 1997; Talling et al., 2012). Decimeter- to meter-scale depositional relief above the debrites impacted routing of subsequent turbidity currents, with denser parts of flows depositing and onlapping the relief, whereas less-dense parts of the flows bypassed down-dip into the basin (e.g. Pickering and Corregidor, 2000; Armitage et al., 2009; Kneller et al., 2016).

Megabeds

MT-4

Description.--- The MT-4 marker bed (Fig. 2) comprises a tripartite structure in the field area (Figs. 8 and 10), from base to top: 1) a debritic division; 2) a calcareous, graded sandstone division; 3) a mudstone division. The debritic division is matrix supported, which consists of poorly-sorted mudstone, siltstone and sandstone, with infrequent *Nummulite* shells. Clasts within the debritic division vary from millimeter- to meter-scale. Clast shape is variable: sandstone and limestone cobbles are up to 20 cm in diameter; contorted mudstone rafts can be meters in length; rafts of sandstone and limestone (rich in shallow-marine foraminifera) can be up to several meters in length, and are often folded and sheared. Clast size decreases over 10s km from northwest to southeast, where the debritic division pinches out (Fig. 10). The calcareous-sandstone division has a sharp erosional base, and consists of multiple amalgamated beds that form an overall normal grading from very coarse- to very-fine sandstone. The transition from the calcareous-sandstone into the mudstone division is normally-graded over approximately 0.3 – 0.8 m.

Interpretation.--- Thick beds with this character have been termed 'megabeds'. Megabeds in the Jaca Basin have been interpreted as "megaturbidites", or "megabreccias" (Puigdefàbregas et al., 1975; Rupke, 1976; Johns et al., 1981; Labaume et al., 1987; Rosell and Wiezorek, 1989; Mutti, 1992; Payros et al., 1999); however the term megaturbidite implies a singular transport process which is misleading (e.g. Bouma, 1987). Therefore, herein the term "megabed" will be used. Megabeds in the Jaca Basin are traditionally thought to be deposited by bi-partite gravity flows consisting of: 1) a basal grain- or debris-flow; 2) an upper, turbulent flow (Rupke, 1976; Labaume et al., 1983; Puigdefàbregas, 1986; Rosell and Wiezorek, 1989; Mutti et al., 1999; Payros et al., 1999). Megabeds have been also interpreted to be similar to hybrid beds as they contain divisions deposited by both laminar and turbulent flows (Haughton et al., 2009; Fallgatter et al., 2016). The lateral facies changes observed (see also: Rupke, 1976; Johns et al., 1981; Labaume et al., 1987; Rosell and Wiezorek, 1989; Payros et al., 1999) imply that the relative importance of particular depositional processes varies across the basin, notably an increase in the thickness of the turbidite division with respect to the basal debrite division towards the southeast. This may show the ability of the turbidity current to more easily surmount topography, compared to debris flows, and flow farther up the regional dip-slope into proximal parts of the basin relative to the clastic system (e.g. Muck and Underwood, 1990; Al Ja'aidi, 2000; Al Ja'aidi et al., 2004; Bakke et al., 2013). The distinctive facies of MT-4, and the ability to map it reliably over 70 km southeast to northwest, make it a marker bed that is confidently used to correlate turbidite packages between outcrops.

Paleocurrents

Throughout the field area, sole structures indicate paleoflow to the northwest, which is consistent with published data (Figs. 9A, B; Rupke, 1976; Mutti, 1977; Mutti, 1992; Remacha and

Fernández, 2003), and defines the approximate direction of depositional dip. Ripple cross-lamination is rare in proximal localities; where present it occurs on bed tops and indicates paleoflow to the northwest. In distal localities, ripple crests occur on the upper surface of D1 of hybrid beds and indicate paleoflow to the north (Figs. 9A and 9B), which is also consistent with previous studies (Remacha and Fernández, 2003; Remacha et al., 2005).

Facies variability and geometry

Proximal localities

Proximal facies variability and package geometries are documented in a depositional dip-oriented correlation panel (W–W`; Fig. 10) and two strike-oriented correlation panels (X-X` Figs. 3B, 12; 1.25 and 2 km-long; minimum distance due to shortening). At least 6 sandstone-prone lobes separated by fine-grained and/or thin-bedded packages are identified in the proximal area of the basin between Fanlo 2 and Yésero; Lobes 1 – 6 (Figs. 10, 12).

Lobe 1 immediately overlies Db-1 and is 2.5 – 6 m thick, (Figs. 8, 10, 12). Lobe 1 comprises thick-bedded sandstones in southeastern sections at Fanlo 2 and Fanlo 1 (Fig. 3). Eleven kilometers down-dip to the northwest, Lobe 1 transitions to medium-bedded sandstone facies at Linás de Broto, and to thin-bedded facies 3.5 km further down-dip at Yésero 2 (Fig. 10). Lobe 1 is sandstone-prone and is of broadly consistent thickness at all localities, even with variable underlying topography created by Db-1. Onlap at a decimeter- to meter-scale is locally present and is typically associated with large clasts in the underlying Db-1 (Fig. 8).

Lobe 2 is 0.5 – 3 m thick and comprises thick-bedded sandstone facies at Fanlo 2 and Fanlo 1 and transitions to thin-bedded facies at Linás de Broto (Fig. 3). Across depositional-strike, Lobe 2 scours into Lobe 1 and intervening thin-beds at Fanlo Track (Fig. 12). Further north, Lobe 2 thins and fines northward, and pinches out between A Lecina and El Bano (Fig. 12).

Lobe 3 thickens from 2.25 m of thick-bedded sandstone facies at Fanlo 2 to 4.25 m at Fanlo 1, with a concomitant increase in thin- and medium-bedded facies. Lobe 3 then thins northwest to Linás de Broto (Fig. 10). North of Fanlo 1, across depositional-strike, Lobe 3 thins to 3 m of medium-bedded sandstone facies at Fanlo Track before pinching out between A Lecina and El Bano (Fig. 12).

Lobe 4 is best exposed at El Bano (Figs. 3, 12) where it comprises 4 m of medium- and thin-bedded sandstone facies. The lobe thins and fines to the south at A Lecina before pinching out south of Fanlo Track (Figs. 3, 12), and as such is not recorded in Figures 8 and 10. The thinning of Lobe 4 to the south, and its distribution of facies associations, suggest that its main depocenter lay to the north of El Bano (Figs. 3, 12).

Lobe 5 is subdivided into Lobe 5a and 5b in the El Chate cliff section (Fig. 8), where a thin-bedded package separates them; the two packages are grouped together elsewhere due to challenges in differentiating them at several locations. At Fanlo 2, Lobe 5 is a 9.5 m thick package of thick-bedded sandstones intercalated with medium- and thin-bedded sandstones (Figs. 8, 10). Lobe 5 is 10.25 m thick at Fanlo 1. Lobe 5a is 4 m thick and consists of thick-bedded sandstone facies. Lobe 5b is 6.25 m thick and consists of medium- and thin-bedded sandstone facies. Lobe 5 thins to 3 m down-dip at Linás de Broto (Figs. 3, 10). Across-strike to the north of Fanlo 1, Lobe 5 thins and fines laterally into a thin-bedded interval at Fanlo Track (Figs. 3, 12), and is no longer observed in A Lecina (Fig. 12).

Lobe 6 stratigraphically underlies MT-4, and is best exposed in the cliffs of the Barranco El Chate valley (Figs. 3, 8, 12). There, Lobe 6 abruptly thickens from a <1 m-thick thin-bedded package at El Chate Cliffs (Figs. 8D, 12) into a 9 m-thick, thick-bedded sandstone package at Barranco El Chate 1 km to the west (Fig. 12). The Lobe 6 package consists of thick- and medium-bedded sandstones at Fanlo Track, A Lecina and El Bano (Fig. 12). Across depositional-strike from Barranco El Chate, Lobe 6 thins to ~3 m of thin-bedded sandstone northwards at Buesa (Fig. 12). Physical correlation to Linás de Broto and Yésero (1 and 2) is not possible; however Lobe 6 is represented by one of the thin-bedded intervals immediately below MT-4. The base of Lobe 6 is typically scoured in the El Chate cliffs (Fig. 8), and the Barranco El Chate and Fanlo Track logged sections. Lobe 6 does not crop out at Fanlo 1 (Figs. 8, 12).

The distinctive scoured base to Lobe 6 is present to the south, north and west of Fanlo 1 (Fig. 8), which implies this locality represents a fine-grained sediment bypass-dominated zone (e.g. Stevenson et al., 2015). An alternative explanation is that Lobe 6 shows a lateral facies change to a thin-bedded, fine-grained package at Fanlo 1. However, this is not preferred as the facies would have to transition from relatively thick-bedded to thin-bedded and back to thick-bedded (El Chate Cliffs to Fanlo 1 to Fanlo Track), which is not commonly observed in lobes over short distances. The across-strike geometry of the resultant deposit from the El Chate Cliffs to Fanlo Track implies the updip portion of the lobe has a "finger-like" geometry akin to those described from distal fringe deposits (e.g. Groenenberg et al., 2010).

Medial localities

Medial localities are typified by the Acín locality, approximately 20 km down-dip of the Yésero 2 locality (Figs. 3, 10). MT-4 constrains the stratigraphy, and in the absence of evidence of significant erosion, indicates that the deposits here are quasi-contemporaneous with those in proximal localities (Fanlo 2 to Yésero, Fig. 3). Four sharp-based and sharp-topped sandstone-prone packages in the section (Ac1-4; 4-7 m thick), which comprise thick-, medium- and thin-bedded sandstones, separated by 10s cm- to m-scale thin-bedded or mudstone-prone intervals (Fig. 10), are interpreted as lobes. Bed types are dominated by high- and low-concentration turbidity current deposits; hybrid beds make-up only 2% of beds (Fig. 11A). The Ac1-4 sandstone lobes are generally thicker, thicker-bedded and coarser-grained than the sandstone lobes observed up-dip at the Linás de Broto and Yésero 2 localities.

Distal localities

Four sections were logged in a down-dip transect between the villages of Aragüés del Puerto and Ansó, and two in across-strike positions at Ansó and Hecho (Figs. 3, 10, 13). The studied stratigraphy, previously described in Remacha and Fernández, (2003), is correlated using the MT-4 megabed. The proportion and cumulative thickness of hybrid beds increases abruptly from Acín to Aragüés del Puerto (Figs. 10, 11A; see also: Remacha and Fernández, 2003), but decreases northwards from Hecho South to Hecho North over 1 km (Figs. 3, 11B, 13). Sandstone bed thicknesses and grainsize do not change significantly from proximal areas (see also Remacha et al., 2005). However, total bed thicknesses do increase as D3 and D4 are developed in distal localities, and mudstone caps are also thicker (see also Remacha et al., 2005). Hummock-type bedforms and convolute ripple cross-laminations are identified in distal localities, in both turbidites and hybrid beds (Fig. 6).

Typically, beds and packages of beds (of similar thicknesses and facies) show significant changes in bed thickness, grain-size and sedimentary textures on a km-scale between localities and are challenging to correlate (Figs. 10, 13). Hybrid beds can be highly variable in character over 100s-m (e.g. Fonnesu et al., 2015); therefore caution is needed when correlating beds based on facies alone. Only Beds 1 (3.2 m thick), 2 (3 m thick) and 3 (1.2 m thick) are tentatively correlated between localities in a down-dip direction (Fig. 10). There is ~3 m of relatively thin-bedded stratigraphy between beds 1 and 2, which is consistent between localities in a down-dip orientation. However, Beds 1 and 2 are less correlatable across strike on a 100s- to 1000's-m scale (Fig. 13). There is a general northward bed-thinning over 400 m at Ansó, whereas from Hecho South to Hecho North (~1 km) Beds 1-3 appear less distinctive (Figs. 3, 13). The proportion of hybrid beds also decreases and D6 is less common, indicating major bed-scale variability over relatively short distances (although potentially tectonically shortened by ~30%; Teixell and García-Sansegundo, 1995).

Discussion

Process transformations and products of flow deflection

Evidence and origin of flow deflection.--- Documented paleocurrent trends suggest variability in flow direction during single events (Fig. 9A, B). The consistent west/northwest orientation of sole structures indicates the primary direction of the lower/earlier flow-components. By contrast, the ripple cross-lamination suggests that the upper/later flow-components (deflected flow) flowed northwards. This suggests that the primary and deflected parts of the flows were divergent (see also: Remacha et al., 2003; Remacha et al., 2005). Paleogeographic reconstructions of the Jaca Basin suggest a narrowing of the basin westward of Jaca, which is attributed to the development of axial thrust sheets and the influence of the Pamplona Fault that separated the Jaca Basin from the Basque Basin to the northwest (e.g. Mutti, 1985; Puigdefàbregas and Souquet, 1986; Puigdefàbregas et al., 1992; Payros et al., 1999; Remacha and Fernández, 2003). Distal narrowing of the basin likely caused an increase in flow interactions with basin margin slopes. Higher concentration parts of flows were strongly confined and “steered” by basinal topography (e.g. Muck and Underwood, 1990; Al Ja’aidi, 2000; McCaffrey and Kneller, 2001; Sinclair and Tomasso, 2002; Amy et al., 2004; Bakke et al., 2013; Stevenson et al., 2014a; Spychala et al., 2017c). In contrast, the upper, more dilute, parts of the flow were able to run up confining slopes and deflect back into the basin to produce paleocurrent indicators divergent to those formed by the basal flow components (e.g. Pickering and Hiscott, 1985; Kneller et al., 1991; Kneller and McCaffrey, 1999; McCaffrey and Kneller, 2001; Hodgson and Haughton 2004; Remacha et al., 2005; Tinterri et al., 2017).

Generation of hybrid beds through flow deflection.--- Hybrid beds have been recognized in a wide range of deep-water sub-environments, and attributed to a variety of depositional processes (e.g. Talling et al., 2004; Baas et al., 2009; Haughton et al., 2009; Hodgson, 2009; Patacci and Haughton, 2014; Hovikoski et al., 2016; Tinterri et al., 2016; Kane et al., 2017). Here, poorly-sorted divisions (D3 and D4) are interpreted to be deposited from predominantly cohesive flows. Common sharp boundaries between different divisions (Fig. 5) imply rheological contrasts within the parent flows (Kane and Pontén, 2012). Instabilities within the flow, which imparted changes in velocity, sediment concentration and fall-out rate, may have been caused by internal waves within the deflected flow (Patacci et al., 2015). Variations in flow concentration and velocity of deflected flows (e.g. Kneller et al., 1991) are likely to promote transitional flow behaviour (e.g. Baas et al., 2009). Disaggregated and folded layers of clasts within D3 and D4 (Fig. 5) are interpreted to be deposited from a flow transitional between turbulent and laminar flow regimes (Fig. 14B; *sensu* Baas et al., 2011). Clasts of similar lithology to underlying divisions are interpreted to have been eroded or entrained into an overriding laminar flow (Fig. 14B; see also: Baas et al., (2011)). Turbulent flow conditions are interpreted to have promoted deposition of relatively clean silts and sands, which were then entrained and carried in laminar flows (Fig. 14B).

Bores within a deflected flow are attributed to the formation of hummock-type bedforms (Pickering and Hiscott, 1985; Remacha et al., 2005; Tinterri et al., 2017), and convolute lamination (Tinterri et al., 2016). The lateral juxtaposition of convolute lamination, hummock-type bedforms, crudely laminated liquefied divisions, and hybrid beds has been interpreted as a continuum of facies formed due to flow deflection (Muzzi Magalhaes and Tinterri, 2010; Tinterri and Tagliaferri, 2015; Tinterri et al., 2016). Hybrid beds deposited from this process response are tripartite, including an overlying laminated division, and are interpreted to form due to flow deceleration against a slope (e.g. Tinterri et al., 2016). Here, the absence of crudely laminated liquefied divisions, and laminated divisions that overlie the poorly sorted divisions (i.e. D3 and D4) suggest hybrid beds formed from the collapse and deflection of an individual flow, which transformed from turbulent to cohesive.

Beds in confined basins with poorly-sorted divisions featuring thin layers of siltstone or sandstone, and/or clasts, which may be present as folded or disaggregated layers, or dispersed through the bed, have also been interpreted to form through liquefaction of beds caused by flow deflection (Pickering and Hiscott, 1985; Remacha and Fernández, 2003; Remacha et al., 2005; Muzzi Magalhaes and Tinterri, 2010). Post-depositional reworking of the clean sandstone divisions (e.g. D1 and D2) by successive internal waves or ‘bores’ have been interpreted to develop fining-upwards divisions of sandstone-mudstone couplets from a progressively waning flow (Pickering and Hiscott, 1985; Remacha et al., 2005; Muzzi Magalhaes and Tinterri, 2010). Liquefaction of beds is attributed to shearing caused by internal waves within the flow (Pickering and Hiscott, 1985; Remacha and Fernández, 2003; Remacha et al., 2005; Muzzi Magalhaes and Tinterri, 2010). This mechanism fails to explain the entrainment of lower divisions into upper divisions observed here (Figs. 5E, F), as liquefaction would promote loading into underlying sediment. Furthermore, the common sharp contacts between divisions (Figs. 5A, B, C, E) imply that no significant liquefaction took place. Trains of bores have also been invoked to explain beds with abrupt contacts between poorly-sorted divisions and mudstone forming through obliteration of primary fabrics (Remacha et al., 2005; Muzzi Magalhaes and Tinterri, 2010). However, we consider this mechanism unlikely as: 1) the most dilute part of the flow would be associated with the strongest bores; 2) no further bores depositing sandstone-mudstone couplets could occur; and 3) thin hybrid beds (e.g. Fig. 5A), deposited from smaller magnitude flows or the dilute lateral fringes of flows, would require strong bores to form in small or dilute flows. The observations are more adequately explained by deposition from cohesive flows.

Role of slope substrate entrainment.--- The increase in the proportion of hybrid beds from proximal to distal localities (Fig. 11), and evidence of flow deflection (Figs. 9A, B), indicate changes in flow behaviour and basin physiography. Slope substrate clasts have been observed in hybrid beds of the Gres d'Annot system (McCaffrey and Kneller, 2001), however, these have not been linked to flow transformation. Here, we suggest that hybrid beds were generated distally within the Jaca Basin by flows interacting with the southern carbonate slope (Fig. 14). This interpretation is underpinned by 3 lines of evidence:

1) Frontal and lateral lobe fringes in proximal and medial locations (Fig. 3) lack hybrid beds, whereas they become significantly more abundant to the northwest of Acín (Figs. 10, 11). This suggests the location of flow transformation lay northwest (basinward) of Acín. In distal locations, the northward

decrease in hybrid bed prevalence and thickness, for example from Hecho South to Hecho North (Figs. 11B, 13), suggests a local control on the development of hybrid beds.

2) Here, a ripple or wavy laminated division (D2) is identified above D1 (Fig. 5), which is normally occupied by banded or muddy sandstone in conventional hybrid bed models (e.g. Haughton et al., 2009). Ripple and hummock-type bedforms are indicative of flows that tractionally reworked the bed (e.g. Walker, 1967; Allen, 1982; Southard, 1991; Remacha et al., 2005; Sumner et al., 2008; Baas et al., 2009; Tinterri et al., 2016), suggesting D2 is a product of a separate or later flow-component (Fig. 14). The deposition of D2 prior to the deposition of D3 and D4 suggests the deflected flows were longitudinally segregated (Fig. 14), with a forerunning turbulent flow-component that reworked the D1 deposits. This was followed by deposition of laminar or transitional flow-components that deposited D3 and D4.

3) The presence of D6 (Fig. 5) is interpreted to reflect substrate entrainment from the carbonate-rich southern slope, which shares mineralogical and biogenic content with carbonate observed in D6 (Mutti et al., 1972; Cámara and Klimowitz, 1985; Remacha et al., 2005). An alternative explanation is that the carbonate enrichment of flows occurred across the basin, or that D6 represents a hemipelagic drape (Mutti et al., 1972; Rupke, 1976; Mutti, 1977). A local origin of D6 is inferred as the absence of D6 in proximal and medial localities (Fig. 10) would require either: 1) D6 to be eroded by every subsequent flow; or 2) the flow responsible bypassed in these localities in every case, which we consider implausible. The more-common occurrence of D6 in hybrid beds compared to turbidites, suggests that deflected flows entrained carbonate mud substrate, whereas a hemipelagic drape should be present in both hybrid beds and turbidites (see also: Remacha et al., 2005). Furthermore, the common normal-grading of D5 into D6 suggests a turbiditic origin where terrigenous and carbonate clay was hydraulically fractionated within the dilute parts of flows (Remacha et al., 2005).

In most basins featuring hybrid beds, the source of clay driving flow transformation can only be inferred (see also: Fonnesu et al., 2016), as the type of intrabasinal clay is similar to that in the flow, making it challenging or impossible to distinguish in outcrop or core. Here, D6 acts as a distinctive 'tracer' near the location of flow transformation. This demonstrates that flow transformation can occur as a result of flows entraining substrate as they deflect off intrabasinal slopes in confined settings.

Contemporaneous systems with different stacking patterns

Spatially Distinct Stacking Patterns.--- Stacking patterns within the Upper Broto System have been described as tabular, where proximal and medial sheet-like lobes transition to the individual bed-scale stacking of the basin-plain environment (Mutti et al., 1999; Remacha and Fernández, 2003; Tinterri et al., 2003). However, the evidence outlined in this work suggests that individual bed correlation in both proximal and distal localities is, at best, challenging (see also Mutti, 1992). Stratigraphic changes in bed stacking patterns are attributed to changing confinement as a basin fills (e.g. Hodgson and Haughton, 2004; Marini et al., 2015; Fonnesu et al., 2018; Liu et al., 2018). Here, different lobe stacking styles are described within the same stratigraphic interval, and interpreted to reflect different flow processes and depositional architectures from proximal to distal localities (see also: Fonnesu et al., 2018).

Lobes are identified in proximal localities based on their geometries, facies, and facies transitions (Figs. 10; 12). The lateral and longitudinal offset of thick-bedded sandstone facies indicates the depocentre of successive lobes moved away from the depositional relief of previous lobes, and stacked in a compensational manner (Figs. 12, 15B; e.g. Mutti and Sonnino, 1981; Parsons et al., 2002; Deptuck et al., 2008; Prélat et al., 2009; Marini et al., 2015; Picot et al., 2016). The identification of lobes medially within the basin, and bypass-dominated facies proximally, indicates some lobes are the products of flows that bypassed proximal localities (Fig. 15). These interpretations are supported by longitudinal and lateral facies and thickness changes within the lobes identified (Figs. 10, 12).

In distal localities, beds do not form clear packages with lobate geometries as they do in proximal and medial locations (Fig. 13). Similarly, they do not exhibit persistent lateral and longitudinal trends in thickness and facies (e.g. lobe axis to lobe fringe) observed in proximal localities, and in other basins (e.g. Mutti and Sonnino, 1981; Prélat et al., 2009; Grundvåg et al., 2014; Marini et al., 2015; Spychala et al., 2017a). Some anomalously thick beds can be tentatively correlated (Fig. 10). However, it is not possible to confidently correlate most beds across these areas, particularly across depositional-strike (Fig. 13B; *c.f.* Remacha and Fernández, 2003), suggesting beds may not be as tabular as previously suggested.

The outcrop belt is slightly oblique to the primary paleocurrent direction, and therefore some changes in architecture could be attributed to across depositional-strike facies variations. However, irrespective of individual bed correlations and outcrop belt orientation, this study recognizes differences in facies and stacking patterns between proximal, medial, and distal localities. The marked distribution of facies, bed types, and stacking patterns indicates a basinal control. The implications of these differences are that fundamentally different stacking styles can occur within the same stratigraphic interval of deep-water systems in confined basins.

A similar distribution of facies is observed in the Gottero Sandstone, Italy. Proximal localities are characterized by lobes, whereas distal localities comprise thick, basin-wide, tabular turbidites and hybrid beds in these basins (Fonnesu et al., 2018). It is interpreted that regular-sized flows were relatively unconfined and formed proximal lobes, whereas large flows bypassed proximal localities (see also: Wynn et al., 2002; Remacha et al., 2005), entrained large rafts of substrate, and deposited thick basin-wide turbidites and hybrid beds (Fonnesu et al., 2018). The distal deposits of the Upper Broto do not exhibit evidence of significant basin-floor erosion and entrainment, suggesting highly energetic flows were not present. Some anonymously thick beds (1 – 3.2 m) in the Upper Broto could be associated with larger volume flows into the basin (e.g. Remacha et al., 2005); however, the vast majority of beds are thinner than 1 m (Figs. 10, 13). Bed thickness increases in the Upper Broto are predominantly facilitated by the development of hybrid beds, the thickness of which are shown to be highly variable and strongly controlled by local topography (e.g. Sumner et al., 2012; Fonnesu et al., 2015). Therefore, it is suggested that facies distribution and hybrid bed emplacement are predominantly controlled by flows interacting with a confining slope (Fig. 15), which does not necessitate, but does not preclude, larger flows.

The Effect Of Deflected-Flows On Stacking Patterns.--- Hybrid beds, up to 3.2 m-thick (post-compaction; Fig. 10), which thin and decrease in abundance away from the slope (Figs. 11B, 13; in this case, from south to north; see also Amy et al., (2004)), are present in distal localities. These beds could have created, and/or healed, significant 3D topography on the contemporaneous seabed, influencing the routing of subsequent events (e.g. Remacha et al., 2005; Figs. 15C, 16). Beds with relatively thick mudstone caps are often associated with flow ponding (e.g. Pickering and Hiscott, 1985; Haughton, 1994; Remacha et al., 2005; Muzzi Magalhaes and Tinterri, 2010), suggesting some flows deposited in bathymetric lows. Flows were deflected near perpendicular to the main paleocurrent of the primary flows, causing deflected-flow deposits to develop geometries and facies tracts perpendicular to those of the primary deposits (Figs. 15C, 16). This may have resulted in complicated 3D bed geometries, which can overlap the stacking pattern of the primary flow deposits (Figs. 15C, 16). This subtle topography was likely felt by the flows and drove deposition in the inherited topographic lows, developing complex bed-scale compensation patterns (Fig. 16).

Conclusions

Well-constrained outcrops along a 70 km dip-orientated transect of an exhumed deep-water depositional system permit proximal to distal analysis of facies and stacking patterns. Contemporaneous but contrasting stacking pattern within the same stratigraphic interval is described in detail for the first time. Proximal localities are characterized by sandstone-rich lobes interpreted to stack compensationally. Distal localities are characterized by interbedded comparatively tabular clean sandstones and hybrid beds which neither stack to form lobes, nor form well-defined tabular sheets.

Here, we present a system that generated hybrid bed through interaction with an intrabasinal confining slope. In most basins featuring hybrid beds, the source of clay responsible for flow transformation can only be inferred as the clay in the flow is compositionally similar to the clay present on the basin-floor. Here, a locally derived and distinct carbonate mud lithofacies demonstrates that entrainment of substrate from an adjacent slope is capable of causing flow transformation. The localized development of hybrid beds through entrainment of slope mud could create depositional relief that influenced flow behavior and deposit geometries, resulting in depositional architectures that diverge from traditional models of either lobe or tabular-sandstone stacking patterns. The co-development of different stacking patterns in the same stratigraphic interval suggests that a false dichotomy of lobes *versus* sheets to characterize basin-floor architectures could exist, and that the stratigraphic and process record of their transitions merit future investigations to better our understanding of submarine fan architecture.

Acknowledgments

The AAPG Foundation Grants-in-Aid Program is thanked for providing funding towards the study. Lewis Burden and Bonita Barrett are thanked for their collaboration and assistance in the field. We wish to thank Gary Hampson and Steve Hubbard for their editorial handling of the manuscript. Julian Clark and Roberto Tinterri are thanked for their thorough and constructive reviews which greatly enhanced the clarity of the manuscript.

References

Al Ja'aidi, O.S., 2000, The influence of topography and flow efficiency on the deposition of turbidites: PhD thesis, University of Leeds, 162 p.

Al Ja'aidi, O.S., McCaffrey, W.D., and Kneller, B.C., 2004, Factors influencing the deposit geometry of experimental turbidity currents: implications for sand-body architecture in confined basins, *in*

Lomas, S.A. and Joseph, P. eds., Confined Turbidite Systems, Geological Society, London, Special Publications, London, v. 222 p. 45–58.

Allen, J.R.L., 1982, Sedimentary structures, Vol. 1-2.: Elsevier, Amsterdam.

Amy, L.A., McCaffrey, W.D., and Kneller, B.C., 2004, The influence of a lateral basin-slope on the depositional patterns of natural and experimental turbidity currents, *in* Joseph, P. and Lomas, S.A. eds., Deep-Water Sedimentation in the Alpine Basin of SE France. New perspectives on the Gres d'Annot and related systems., Geological Society, London, Special Publications, v. 221, p. 311–330.

Amy, L.A., Kneller, B.C., and McCaffrey, W.D., 2007, Facies architecture of the Gres de Peira Cava, SE France: landward stacking patterns in ponded turbiditic basins: Journal of the Geological Society, v. 164, p. 143–162, doi: 10.1144/0016-76492005-019.

Armitage, D.A., Romans, B.W., Covault, J.A., and Graham, S.A., 2009, The Influence of Mass-Transport-Deposit Surface Topography on the Evolution of Turbidite Architecture: The Sierra Contreras, Tres Pasos Formation (Cretaceous), Southern Chile: Journal of Sedimentary Research, v. 79, no. 5, p. 287–301, doi: 10.2110/jsr.2009.035.

Baas, J.H., Best, J.L., Peakall, J., and Wang, M., 2009, A phase diagram for turbulent, transitional, and laminar clay suspension flows: Journal of Sedimentary Research, v. 79, no. April, p. 162–183, doi: 10.2110/jsr.2009.025.

Baas, J.H., Best, J.L., and Peakall, J., 2011, Depositional processes, bedform development and hybrid bed formation in rapidly decelerated cohesive (mud-sand) sediment flows. Sedimentology: Sedimentology, v. 58, no. July 2016, p. 1953–1987, doi: 10.1111/j.1365-3091.2011.01247.x.

Baas, J.H., Davies, A.G., and Malarkey, J., 2013, Bedform development in mixed sand – mud : The contrasting role of cohesive forces in flow and bed: Geomorphology, v. 182, p. 19–32, doi: 10.1016/j.geomorph.2012.10.025.

Bakke, K., Kane, I.A., Martinsen, O.J., Petersen, S.A., Johansen, T.A., Hustoft, S., Jacobsen, F.H., and Groth, A., 2013, Seismic modeling in the analysis of deep-water sandstone termination styles: AAPG Bulletin, v. 97, no. 5020, p. 1395–1419, doi: 10.1306/03041312069.

Barnes, N.E., and Normark, W.R., 1985, Diagnostic parameters for comparing modern submarine fans and ancient turbidite systems, *in* Bouma, A.H., Normark, W.R., and Barnes, N.E. eds., Submarine fans and related turbidite systems, Springer New York, New York, NY, p. 13–14.

Barnolas, A., and Teixell, A., 1994, Platform sedimentation and collapse in a carbonate-dominated margin of a foreland basin (Jaca basin, Eocene, southern Pyrenees): Geology, v. 22, no. 12, p. 1–4.

Bayliss, N.J., and Pickering, K.T., 2015, Deep-marine structurally confined channelised sandy fans: Middle Eocene Morillo System, Ainsa Basin, Spanish Pyrenees: Earth Science Reviews, v. 144, p. 82–106, doi: 10.1016/j.earscirev.2014.11.014.

Beaubouef, R.T., 2004, Deep-water leveed-channel complexes of the Cerro Toro Formation, Upper Cretaceous, southern Chile: AAPG Bulletin, v. 88, no. 11, p. 1471–1500, doi: 10.1306/06210403130.

Best, J.L., and Bridge, J.S., 1992, The morphology and dynamics of low amplitude bedwaves upon upper stage plane beds and the preservation of planar laminae : Sedimentology, v. 39, p. 737–752, doi: 10.1111/j.1365-3091.1992.tb02150.x.

Bouma, A.H., 1987, Megaturbidite: An acceptable term? Geo-Marine Letters, v. 7, no. 2, p. 63–67, doi: 10.1007/BF02237985.

Butler, R.W.H., and Tavarnelli, E., 2006, The structure and kinematics of substrate entrainment into high-concentration sandy turbidites: a field example from the Gorgoglione “flysch” of southern Italy: Sedimentology, v. 53, no. 3, p. 655–670, doi: 10.1111/j.1365-3091.2006.00789.x.

Caja, M.A., Marfil, R., Garcia, D., Remacha, E., Morad, S., Mansurbeg, H., Amorosi, A., Martínez-Calvo, C., and Lahoz-Beltrá, R., 2010, Provenance of siliciclastic and hybrid turbiditic arenites of the

Eocene Hecho Group, Spanish Pyrenees: Implications for the tectonic evolution of a foreland basin: Basin Research, v. 22, no. 2, p. 157–180, doi: 10.1111/j.1365-2117.2009.00405.x.

Cámara, P., and Klimowitz, J., 1985, Interpretación geodinámica de la vertiente centro-occidental surpirenaica (cuencas de Jaca-Tremp): Estudios geológicos, v. 41, no. 5-6, p. 391–404.

Cartapanis, O., Bianchi, D., Jaccard, S.L., and Galbraith, E.D., 2016, Global pulses of organic carbon burial in deep-sea sediments during glacial maxima: Nature Communications, v. 7, p. 10796.

Cartigny, M.J.B., Eggenhuisen, J.T., Hansen, E.W.M., and Postma, G., 2013, Concentration-dependent flow stratification in experimental high-density turbidity currents and their relevance to turbidite facies models: Journal of Sedimentary Research, v. 83, p. 1046–1064, doi: 10.2110/jsr.2013.71.

Clark, J.D., and Pickering, K.T., 1996, Architectural elements and growth patterns of submarine channels: Application to hydrocarbon exploration: AAPG Bulletin, v. 80, p. 194–221, doi: 10.1306/64ED878C-1724-11D7-8645000102C1865D.

Clark, J.D., Puigdefàbregas, C., Castelltort, S., and Fildani, A., 2017, Propagation of Environmental Signals within Source-to-Sink Stratigraphy, SEPM Field Trip Guidebook 13, p. 1–63.

Das Gupta, K., and Pickering, K.T., 2008, Petrography and temporal changes in petrofacies of deep-marine Ainsa – Jaca basin sandstone systems, Early and Middle Eocene, Spanish Pyrenees: Sedimentology, v. 55, no. 4, p. 1083–1114, doi: 10.1111/j.1365-3091.2007.00937.x.

Deptuck, M.E., Piper, D.J.W., Savoye, B., and Gervais, A., 2008, Dimensions and architecture of late Pleistocene submarine lobes off the northern margin of East Corsica: Sedimentology, v. 55, p. 869–898.

Dreyer, T., Corregidor, J., Arbues, P. and Puigdefabregas, C., 1999. Architecture of the tectonically influenced Sobrarbe deltaic complex in the Ainsa Basin, northern Spain. Sedimentary Geology, 127(3-4), pp.127-169.

Eggenhuisen, J.T., McCaffrey, W.D., Haughton, P.D.W., and Butler, R.W.H., 2011, Shallow erosion beneath turbidity currents and its impact on the architectural development of turbidite sheet systems: Sedimentology, v. 58, no. 4, p. 936–959, doi: 10.1111/j.1365-3091.2010.01190.x.

Elliott, T., 2000, Megaflute erosion surfaces and the initiation of turbidite channels: Geology, v. 28, no. 2, p. 119–122, doi: 10.1130/0091-7613(2000)28<119:MESATI>2.0.CO;2.

Fallgatter, C., Kneller, B., Paim, P.S.G., and Milana, J.P., 2016, Transformation, partitioning and flow-deposit interactions during the run-out of megaflows: Sedimentology, doi: 10.1111/sed.12307.

Fernández, O., Muñoz, J.A., Arbués, P., Falivene, O., and Marzo, M., 2004, Three-dimensional reconstruction of geological surfaces: An example of growth strata and turbidite systems from the Aínsa basin (Pyrenees, Spain): AAPG Bulletin, v. 88, no. 8, p. 1049–1068, doi: 10.1306/02260403062.

Fonnesu, M., Haughton, P., Felletti, F., and McCaffrey, W., 2015, Short length-scale variability of hybrid event beds and its applied significance: Marine and Petroleum Geology, v. 67, no. May, p. 583–603, doi: 10.1016/j.marpetgeo.2015.03.028.

Fonnesu, M., Patacci, M., Haughton, P.D.W., and Felletti, F., 2016, Hybrid event beds generated by local substrate delamination on a confined-basin floor: Journal of Sedimentary Research, v. 86, no. August, p. 929–943.

Fonnesu, M., Felletti, F., Haughton, P.D.W., Patacci, M., Mccaffrey, W.D., and Mangiagalli, V., 2018, Hybrid event bed character and distribution linked to turbidite system sub-environments: The North Apennine Gottero Sandstone (north-west Italy): Sedimentology, v.65, no. 1, p. 151–190 doi: 10.1111/sed.12376.

Gardner, M.H., Borer, J.M., Melick, J.J., Mavilla, N., Dechesne, M., and Wagerle, R.N., 2003, Stratigraphic process-response model for submarine channels and related features from studies of

Permian Brushy Canyon outcrops , West Texas: Marine and Petroleum Geology, v. 20, p. 757–787, doi: 10.1016/j.marpetgeo.2003.07.004.

Gladstone, C., Stephen, R., and Sparks, J., 2002, The Significance of Grain-Size Breaks in Turbidites and Pyroclastic Density Current Deposits: Journal of Sedimentary Research, v. 72, no. 1, p. 182–191.

Groenenberg, R.M., Hodgson, D.M., Prélat, A., Luthi, S.M., and Flint, S.S., 2010, Flow-deposit interaction in submarine lobes: insights from outcrop observations and realizations of a process-based numerical model: Journal of Sedimentary Research, v. 80, no. 3, p. 252–267, doi: 10.2110/jsr.2010.028.

Grundvåg, S.A., Johannessen, E.P., Helland-Hansen, W., and Plink-Bjölrklund, P., 2014, Depositional architecture and evolution of progradationally stacked lobe complexes in the Eocene Central Basin of Spitsbergen: Sedimentology, v. 61, no. 2, p. 535–569, doi: 10.1111/sed.12067.

Gwiazda, R., Paull, C.K., Ussler, W., and Alexander, C.R., 2015, Evidence of modern fine-grained sediment accumulation in the Monterey Fan from measurements of the pesticide DDT and its metabolites: Marine Geology, v. 363, p. 125–133, doi:https://doi.org/10.1016/j.margeo.2015.02.006.

Harms, J.C., Southard, J.B., Spearing, D.R. and Walker, R.G. 1975 Depositional environments as interpreted from primary sedimentary structures and stratification sequences. Society of Economic Paleontologists and Mineralogists, Short Course 2, 161p.

Haughton, P.D.W., 1994, Deposits of deflected and ponded turbidity currents, Sorbas Basin, Southeast Spain: Journal of Sedimentary Research, v. 64, p. 233–246, doi: 10.1306/D4267D6B-2B26-11D7-8648000102C1865D.

Haughton, P.D.W., Barker, S.P., and McCaffrey, W.D., 2003, Linked debrites in sand-rich turbidite systems - origin and significance: Sedimentology, v. 50, no. 3, p. 459–482, doi: 10.1046/j.1365-3091.2003.00560.x.

Haughton, P.D.W., Davis, C., McCaffrey, W., and Barker, S., 2009, Hybrid sediment gravity flow deposits – Classification, origin and significance: Marine and Petroleum Geology, v. 26, no. 10, p. 1900–1918, doi: 10.1016/j.marpetgeo.2009.02.012.

Hesse, R., 1964, Herkunft und transport der sedimente im bayerischen flyschtrog: Zeitschrift der Deutschen Geologischen Gesellschaft, p. 403–426.

Hirayama, J., and Nakajima, T., 1977, Analytical study of turbidites, Otadai Formation, Boso Peninsula, Japan: Sedimentary Geology, v. 24, no. 6, p. 747–779.

Hodgson, D.M., 2009, Distribution and origin of hybrid beds in sand-rich submarine fans of the Tanqua depocentre, Karoo Basin, South Africa: Marine and Petroleum Geology, v. 26, no. 10, p. 1940–1956, doi: 10.1016/j.marpetgeo.2009.02.011.

Hodgson, D.M., and Haughton, P.D.W., 2004, Impact of syndepositional faulting on gravity current behaviour and deep-water stratigraphy: Tabernas-Sorbas Basin, SE Spain, *in* Lomas, S.A. and Joseph, P. eds., Confined Turbidite Systems, Geological Society, London, Special Publications, p. 135–158.

Hodgson, D.M., Flint, S.S., Hodgetts, D., Drinkwater, N.J., Johannessen, E.P., and Luthi, S.M., 2006, Stratigraphic evolution of fine-grained submarine fan systems, Tanqua Depocenter, Karoo Basin, South Africa: Journal of Sedimentary Research, v. 76, p. 20–40, doi: 10.2110/jsr.2006.03.

Hovikoski, J., Therkelsen, J., Nielsen, L.H., Bojesen-Koefoed, J.A., Nytoft, H.P., Petersen, H.I., Abatzis, I., Tuan, H.A., Phuong, B.T.N., Dao, C.V. and Fyhn, M.B., 2016. Density-flow deposition in a fresh-water lacustrine rift basin, Paleogene Bach Long Vi Graben, Vietnam: Journal of Sedimentary Research, v. 86, no. 9, pp.982-1007.

Iverson, R.M., 1997, The physics of debris flows: Reviews of geophysics, v. 35, no. 3, p. 245–296.

Iverson, R.M., Logan, M., Lahusen, R.G., and Berti, M., 2010, The perfect debris flow? Aggregated results from 28 large-scale experiments: Journal of Geophysical Research: Earth Surface, v. 115, no. F3, doi: 10.1029/2009JF001514.

Jegou, I., Savoye, B., Pirmez, C., and Droz, L., 2008, Channel-mouth lobe complex of the recent Amazon Fan: The missing piece: Marine Geology, v. 252, p. 62–77, doi: 10.1016/j.margeo.2008.03.004.

Jobe, Z.R., Lowe, D.R., and Morris, W.R., 2012, Climbing-ripple successions in turbidite systems: depositional environments, sedimentation rates and accumulation times: Sedimentology, v. 59, no. 3, p. 867–898, doi: 10.1111/j.1365-3091.2011.01283.x.

Johns, D.R., Mutti, E., Rosell, J., and Séguret, M., 1981, Origin of a thick, redeposited carbonate bed *in* Eocene turbidites of the Hecho Group, south-central Pyrenees, Spain: Geology, v. 9, p. 161–164.

Kane, I.A., and Pontén, A.S.M., 2012, Submarine transitional flow deposits in the Paleogene Gulf of Mexico: Geology, v. 40, no. 12, p. 1119–1122, doi: 10.1130/G33410.1.

Kane, I.A., Catterall, V., McCaffrey, W.D., and Martinsen, O.J., 2010, Submarine channel response to intrabasinal tectonics: The influence of lateral tilt: AAPG Bulletin, v. 94, no. 2, p. 189–219, doi: 10.1306/08180909059.

Kane, I.A., Pontén, A.S.M., Vangdal, B., Eggenhuisen, J.T., Hodgson, D.M., and Spychala, Y.T., 2017, The stratigraphic record and processes of turbidity current transformation across deep-marine lobes: Sedimentology, v. 64, no. 5, p. 1236-1273, doi: 10.1111/SED.12346.

Kneller, B., and Branney, M., 1995, Sustained high-density turbidity currents and the deposition of thick massive sands: Sedimentology, v. 42, p. 607–616, doi: 10.1111/j.1365-3091.1995.tb00395.x.

Kneller, B., and McCaffrey, W., 1995, Modelling the effects of salt-induced topography on deposition from turbidity currents, *in* Travis, C.J., Harrison, H., Hudeac, M.R., Vendeville, B.C., Pell, F.J., and Perkins, R.F. eds., Salt, sediment and hydrocarbons, SEPM, 16th Annual Research Conference, p. 137–145.

Kneller, B., and McCaffrey, W.D., 1999, Depositional effects of flow nonuniformity and stratification within turbidity currents approaching a bounding slope; deflection, reflection, and facies variation: Journal of Sedimentary Research, v. 69, no. 5, p. 980–991, doi: 10.2110/jsr.69.980.

Kneller, B., Edwards, D., Mccaffrey, W., and Moore, R., 1991, Oblique reflection of turbidity currents: Geology, v. 19, no. March, p. 250–252.

Kneller, B., Dykstra, M., Fairweather, L., and Milana, J.P., 2016, Mass-transport and slope accommodation: Implications for turbidite sandstone reservoirs: AAPG Bulletin, v. 100, no. 2, p. 213–235, doi: 10.1306/09011514210.

Labaume, P., Mutti, E., Séguret, M., and Rosell, J., 1983, Mégaturbidites carbonatées du bassin turbiditique de l'Eocéne inférieur et moyen sud-pyrénéen: Bulletin de la Société Géologique de France, v. 7, no. 6, p. 927–941, doi: 10.2113/gssgfbull.S7-XXV.6.927.

Labaume, P., Séguret, M., and Seyve, C., 1985, Evolution of a turbiditic foreland basin and analogy with an accretionary prism: Example of the Eocene South-Pyrenean Basin: Tectonics, v. 4, no. 7, p. 661, doi: 10.1029/TC004i007p00661.

Labaume, P., Mutti, E., and Seguret, M., 1987, Megaturbidites: A Depositional model from the Eocene: Geo-Marine Letters, v. 7, no. 2, p. 91–101.

Lowe, D.R., 1982, Sediment gravity flows: II depositional models with special reference to the deposits of high-density turbidity currents: Journal of Sedimentary Research, v. 52, no. 1.

Marini, M., Milli, S., Ravnås, R., and Moscatelli, M., 2015, A comparative study of confined vs. semi-confined turbidite lobes from the Lower Messinian Laga Basin (Central Apennines, Italy): implications for assessment of reservoir architecture: Marine and Petroleum Geology, v. 63, p. 142–165, doi: 10.1016/j.marpetgeo.2015.02.015.

McCaffrey, W., and Kneller, B., 2001, Process controls on the development of stratigraphic trap potential on the margins of confined turbidite systems and aids to reservoir evaluation: AAPG Bulletin, v. 85, no. 6, p. 971–988, doi: 10.1306/8626CA41-173B-11D7-8645000102C1865D.

McClelland, H.L.O., Woodcock, N.H., and Gladstone, C., 2011, Eye and sheath folds in turbidite convolute lamination: Aberystwyth Grits Group, Wales: Journal of Structural Geology, v. 33, no. 7, p. 1140–1147, doi: 10.1016/j.jsg.2011.05.007.

McKie, T., Rose, P.T.S., Hartley, A.J., Jones, D.W., and Armstrong, T.L., 2015, Tertiary deep-marine reservoirs of the North Sea region : an introduction, *in* McKie, T., Rose, P.T.S., Hartley, A.J., Jones, D.W., and Armstrong, T.L. eds., Tertiary deep-marine reservoirs of the North Sea, The Geological Society of London, 403p..

Millán-Garrido, H., Olivia-Urcia, B., and Pocoví-Juan, A., 2006, La transversal de Gavarnie-Guara. Estructura y edad de los mantos de Gavarnie, Guara-Gèdre y Guarga (Pirineo centro-occidental): Geogaceta, v. 40, p. 35–38.

Millington, J.J., and Clark, J.D., 1995, The Charo/Arro Canyon-Mouth Sheet System, South-Central Pyrenees, Spain: A Structurally Influenced Zone of Sediment Dispersal: Journal of Sedimentary Research, v. 65, no. 4, p. 443–454, doi: 10.1306/D426827F-2B26-11D7-8648000102C1865D.

Moody, J.D., Pyles, D.R., Clark, J., and Bouroullec, R., 2012, Quantitative outcrop characterization of an analog to weakly confined submarine channel systems: Morillo 1 member, Ainsa Basin, Spain: AAPG Bulletin, v. 96, no. 10, p. 1813–1841, doi: 10.1306/01061211072.

Muck, M.T., and Underwood, M.B., 1990, Upslope flow of turbidity currents: A comparison among field observations, theory, and laboratory models: Geology, v. 18, no. 1, p. 54–57

Mutti, E., 1977, Distinctive thin-bedded turbidite facies and related depositional environments in the Eocene Hecho Group (South-central Pyrenees, Spain): Sedimentology, v. 24, no. 1, p. 107–131, doi: 10.1111/j.1365-3091.1977.tb00122.x.

Mutti, E., 1984, The Hecho Eocene submarine fan system, south-central Pyrenees, Spain: Geo-Marine Letters, v. 3, no. 2-4, p. 199–202, doi: 10.1007/BF02462468.

Mutti, E., 1985, Turbidite Systems and Their Relations to Depositional Sequences, *in* Zuffa, G.G. ed., Provenance of Arenites, Reidel Publishing Co., Dordrecht, p. 65–93.

Mutti, E., 1992, Turbidite Sandstones: Agip, Istituto di Geologia Università di Parma, Milan.

Mutti, E., and Sonnino, M., 1981, Compensation cycles; a diagnostic feature of turbidite sandstone lobes: International Association of Sedimentologists abstracts; 2nd European regional meeting, p. 120–123

Mutti, E., and Normark, W.R., 1987, Comparing examples of modern and ancient turbidite systems: problems and concepts, *in* Leggett, J.K. and Zuffa, G.G. eds., Marine clastic sedimentology, Springer Netherlands, Dordrecht, p. 1–38.

Mutti, E., Luterbacher, H.P., Ferrer, J., and Rosell, J., 1972, Schema stratigrafico e lineamenti di facies del Paleogene marino della zona centrale sudpirenaica tra Tremp (Catalogna) e Pamplona (Navarra): Memoria della Società Geológica Italiana, v. 11, p. 391–416.

Mutti, E., Séguret, M., and Sgavetti, M., 1988, Sedimentation and deformation in the Tertiary Sequences of the Southern Pyrenees: Field trip 7: University of Parma.

Mutti, E., Tinterri, R., Remacha, E., Mavilla, N., Angella, S., and Fava, L., 1999, An introduction to the analysis of ancient turbidite basins from an outcrop perspective: AAPG Continuing Education Course Note Series 39, 96 p.

Muzzi Magalhaes, P., and Tinterri, R., 2010, Stratigraphy and depositional setting of slurry and contained (reflected) beds in the Marnoso-arenacea Formation (Langhian-Serravallian) Northern Apennines, Italy: Sedimentology, v. 57, no. 7, p. 1685–1720, doi: 10.1111/j.1365-3091.2010.01160.x.

Nardin, T.R., Hein, F.J., Gorsline, D.S., and Edwards, B.., 1979, A Review of mass movement processes, sediment and acoustic characteristics, and contrasts in slope and base-of-slope systems versus canyon-fan-basin floor systems: SEPM Special Publications, , no. 27, p. 61–73.

Nijman, W., and Nio, S.D., 1975, The Eocene Montañana delta (Tremp-Graus Basin, provinces of Lérida and Huesca, southern Pyrenees, N Spain), IX Congrés de Sedimentologie, p. 18

Parsons, J.D., Schweller, W.J., Stelting, C.W., Southard, J.B., Lyons, W.J., and Grotzinger, J.P., 2002, A preliminary experimental study of turbidite fan deposits: Journal of Sedimentary Research, v. 72, p. 839–841, doi: 10.1306/032102720619.

Patacci, M., and Haughton, P.D.W., 2014, Rheological complexity in sediment gravity flows forced to decelerate against a confining slope, Braux, SE France: Journal of Sedimentary Research, v. 84, p. 270–277.

Patacci, M., Haughton, P.D.W., and Mccaffrey, W.D., 2015, Flow behavior of ponded turbidity currents: Journal of Sedimentary Research, v. 85, p. 885–902.

Payros, A., Pujalte, V., and Orue-Etxebarria, X., 1999, The South Pyrenean Eocene carbonate megabreccias revisited: New interpretation based on evidence from the Pamplona Basin: Sedimentary Geology, v. 125, no. 3, p. 165–194, doi: 10.1016/S0037-0738(99)00004-4.

Pickering, K.T., and Hiscott, R.N., 1985, Contained (reflected) turbidity currents from the Middle Ordovician Clotidorme Formation, Quebec, Canada: an alternative to the antidune hypothesis: Sedimentology, v. 32, no. 3, p. 373–394, doi: 10.1111/j.1365-3091.1985.tb00518.x.

Pickering, K.T., and Corregidor, J., 2000, 3D reservoir scale study of Eocene confined submarine fans, south central Spanish Pyrenees, in Deep Water Reservoirs of the World: SEPM, Gulf Coast Section, 20th Annual Bob F. Perkins Research Conference, SEPM, p. 776–781.

Pickering, K.T., and Corregidor, J., 2005, Mass transport complexes and tectonic control on confined basin-floor submarine fans, Middle Eocene, south Spanish Pyrenees: Geological Society, London, Special Publications, v. 244, p. 51–74, doi: 10.1144/GSL.SP.2005.244.01.04.

Pickering, K.T., and Bayliss, N.J., 2009, Deconvolving tectono-climatic signals in deep-marine siliciclastics, Eocene Ainsa basin, Spanish Pyrenees: Seesaw tectonics versus eustasy: Geology, v. 37, no. 3, p. 203–206, doi: 10.1130/G25261A.1.

Picot, M., Droz, L., Marsset, T., Dennielou, B., and Bez, M., 2016, Controls on turbidite sedimentation: Insights from a quantitative approach of submarine channel and lobe architecture (Late Quaternary Congo Fan): Marine and Petroleum Geology, v. 72, p. 423–446, doi: 10.1016/j.marpetgeo.2016.02.004.

Pierce, C.S., Haughton, P.D., Shannon, P.M., Pulham, A.J., Barker, S.P., and Martinsen, O.J., 2018, Variable character and diverse origin of hybrid event beds in a sandy submarine fan system, Pennsylvanian Ross Sandstone Formation, western Ireland: Sedimentology, doi: 10.1111/sed.12412.

Prélat, A., and Hodgson, D.M., 2013, The full range of turbidite bed thickness patterns in submarine lobes: controls and implications: Journal of the Geological Society, v. 170, no. 1, p. 209–214, doi: 10.1144/jgs2012-056.

Prélat, A., Hodgson, D.M., and Flint, S.S., 2009, Evolution, architecture and hierarchy of distributary deep-water deposits: a high-resolution outcrop investigation from the Permian Karoo Basin, South Africa: Sedimentology, v. 56, no. 7, p. 2132–2154, doi: 10.1111/j.1365-3091.2009.01073.x.

Puigdefàbregas, C., 1986, Megaturbidites from the Eocene of Southern Pyrenees: alternative interpretations. AAPG Bulletin, v. 70, 635–636.

Puigdefàbregas, C., and Souquet, P., 1986, Tecto-sedimentary cycles and depositional sequences of the Mesozoic and Tertiary from the Pyrenees: Tectonophysics, v. 129, no. 1, p. 173–203, doi: https://doi.org/10.1016/0040-1951(86)90251-9.

Puigdefàbregas, C., Rupke, N.A., and Sedo, J.S., 1975, The sedimentary evolution of the Jaca Basin. *In*: Rosell, J., Puigdefábregas, C. (Eds.), The sedimentary evolution of the Paleogene South Pyrenean Basin. 9th Congr. Int. Assoc. Sedimentol., Nice, Field-trip 19, part C, 33 pp.

Puigdefàbregas, C., Muñoz, J.A., and Vergés, J., 1992, Thrusting and foreland basin evolution in the Southern Pyrenees, *in* McClay, K.R. ed., Thrust Tectonics, Springer Netherlands, Dordrecht, p. 247–254.

Remacha, E., and Fernández, L.P., 2003, High-resolution correlation patterns in the turbidite systems of the Hecho Group (South-Central Pyrenees, Spain): Marine and Petroleum Geology, v. 20, no. 6, p. 711–726, doi: 10.1016/j.marpetgeo.2003.09.003.

Remacha, E., Gual, G., Bolaño, F., Arcuri, M., Oms, O., Climent, F., Crumeyrolle, P., Fernández, L.P., Vicente, J.C., and Suarez, J., 2003, Sand-rich turbidite systems of the Hecho Group from slope to basin plain; facies, stacking patterns, controlling factors and diagnostic features: Geological field trip 12,.

Remacha, E., Fernández, L.P., and Maestro, E., 2005, The transition between sheet-like lobe and basin-plain turbidites in the Hecho Basin (south-central Pyrenees, Spain): Journal of Sedimentary Research, v. 75, no. 5, p. 798–819, doi: 10.2110/jsr.2005.064.

Ricci-Lucchi, F., 1984, The Deep-Sea Fan deposits of the Miocene Marnoso-arenacea formation, northern Apennines: Geo-Marine Letters, v. 3, no. 1, p. 203–210, doi: 10.1007/BF02462469.

Ricci-Lucchi, F., and Valmori, E., 1980, Basin-wide turbidites in a Miocene, oversupplied deep-sea plain: a geometrical analysis: Sedimentology, v. 27/3, no. 3, p. 241–270, doi: 10.1111/j.1365-3091.1980.tb01177.x.

Rosell, J., and Wiezorek, J., 1989, Main features of megaturbidites in the Eocene of southern Pyrenees: Annales Societatis Geologorum Poloniae, v. 59, p. 3–16.

Rupke, N.A., 1976, Sedimentology of very thick calcarenite-marlstone beds in a flysch succession, southwestern Pyrenees: Sedimentology, v. 23, p. 213–265, doi: 10.1111/j.1365-3091.1976.tb00038.x.

Saller, A., Werner, K., Sugiaman, F., Cebastiant, A., May, R., Glenn, D., and Barker, C., 2008, Characteristics of Pleistocene deep-water fan lobes and their application to an upper Miocene reservoir model, offshore East Kalimantan, Indonesia: AAPG Bulletin, v. 92, no. 7, p. 919–949, doi: 10.1306/03310807110.

Seguret, M., Labaume, P., and Madariaga, R., 1984, Eocene seismicity in the Pyrenees from megaturbidites of the South Pyrenean Basin (Spain): Marine Geology, v. 55, no. 1-2, p. 117–131, doi: 10.1016/0025-3227(84)90136-1.

Sinclair, H.D., and Tomasso, M., 2002, Depositional Evolution of Confined Turbidite Basins: Journal of Sedimentary Research, v. 72, no. 4, p. 451–456, doi: 10.1306/111501720451.

Sohn, Y.K., 2000, Depositional processes of submarine debris flows in the Miocene fan deltas, Pohang Basin, SE Korea with special reference to flow transformation: Journal of Sedimentary Research, v. 70, no. 3, p. 491–503.

Southard, J.B., 1991, Experimental determination of bed-form stability: Annual Review of Earth and Planetary Sciences, v. 19, no. 1, p. 423–455, doi: 10.1146/annurev.ea.19.050191.002231.

Southern, S.J., Patacci, M., Felletti, F., and Mccaffrey, W.D., 2015, Influence of flow containment and substrate entrainment upon sandy hybrid event beds containing a co-genetic mud-clast-rich division: Sedimentary Geology, v. 321, p. 105–122, doi: 10.1016/j.sedgeo.2015.03.006.

Southern, S.J., Kane, I.A., Warchoł, M.J., Porten, K.W., and McCaffrey, W.D., 2017, Hybrid event beds dominated by transitional-flow facies: Character, distribution and significance in the Maastrichtian Springar Formation, north-west Vøring Basin, Norwegian Sea: Sedimentology, v. 64, no. 3, p. 747–776, doi: 10.1111/sed.12323.

Spychala, Y.T., Hodgson, D.M., Prélat, A., Kane, I.A., Flint, S.S., and Mountney, N.P., 2017a, Frontal and lateral submarine lobe fringes: Comparing facies, architecture and flow processes: Journal of Sedimentary Research, v. 87, no. 1, p. 1–21.

Spychala, Y.T., Hodgson, D.M., and Lee, D.R., 2017b, Autogenic controls on hybrid bed distribution in submarine lobe complexes: Marine and Petroleum Geology, v. 88, p. 1078–1093, doi: https://doi.org/10.1016/j.marpetgeo.2017.09.005.

Spychala, Y.T., Hodgson, D.M., and Stevenson, C.J., 2017c, Aggradational lobe fringes: The influence of subtle intrabasinal seabed topography on sediment gravity flow processes and lobe stacking patterns: Sedimentology, v. 64, p. 582–608, doi: 10.1111/sed.12315.

Stevenson, C.J., Talling, P.J., Masson, D.G., Sumner, E.J., Frenz, M., and Wynn, R.B., 2014a, The spatial and temporal distribution of grain-size breaks in turbidites: Sedimentology, v. 61, p. 1120–1156, doi: 10.1111/sed.12091.

Stevenson, C.J., Talling, P.J., Sumner, E.J., Masson, D.G., Frenz, M., and Wynn, R., 2014b, On how thin submarine flows transported large volumes of sand for hundreds of kilometres across a flat basin plain without eroding the sea floor: Sedimentology, p. 1982–2019, doi: 10.1111/sed.12125.

Stevenson, C.J., Jackson, C.A.-L., Hodgson, D.M., Hubbard, S.M., and Eggenhuisen, J.T., 2015, Deep-water sediment bypass: Journal of Sedimentary Research, v. 85, p. 1058–1081, doi: 10.2110/jsr.2015.63.

Straub, K.M., Paola, C., Mohrig, D., Wolinsky, M. A., and George, T., 2009, Compensational stacking of channelized sedimentary deposits: Journal of Sedimentary Research, v. 79, no. 9, p. 673–688, doi: 10.2110/jsr.2009.070.

Sumner, E.J., Amy, L.A., and Talling, P.J., 2008, Deposit structure and processes of sand deposition from decelerating sediment suspensions: Journal of Sedimentary Research, v. 78, no. 8, p. 529–547, doi: 10.2110/jsr.2008.062.

Sumner, E.J., Talling, P.J., and Amy, L. A., 2009, Deposits of flows transitional between turbidity current and debris flow: Geology, v. 37, no. 11, p. 991–994, doi: 10.1130/G30059A.1.

Sumner, E.J., Talling, P.J., Amy, L.A., Wynn, R.B., Stevenson, C.J., and Frenz, M., 2012, Facies architecture of individual basin-plain turbidites: Comparison with existing models and implications for flow processes: Sedimentology, v. 59, p. 1850–1887, doi: 10.1111/j.1365-3091.2012.01329.x.

Sylvester, Z., and Lowe, D.R., 2004, Textural trends in turbidites and slurry beds from the Oligocene flysch of the East Carpathians, Romania: Sedimentology, v. 51, no. 5, p. 945–972, doi: 10.1111/j.1365-3091.2004.00653.x.

Talling, P.J., Amy, L.A., Wynn, R.B., Peakall, J., and Robinson, M., 2004, Beds comprising debrite sandwiched within co-genetic turbidite: origin and widespread occurrence in distal depositional environments: Sedimentology, v. 51, no. 1, p. 163–194, doi: 10.1046/j.1365-3091.2003.00617.x.

Talling, P.J., Amy, L.A., and Wynn, R.B., 2007, New insight into the evolution of large-volume turbidity currents: Comparison of turbidite shape and previous modelling results: Sedimentology, v. 54, no. 4, p. 737–769, doi: 10.1111/j.1365-3091.2007.00858.x.

Talling, P.J., Masson, D.G., Sumner, E.J., and Malgesini, G., 2012, Subaqueous sediment density flows: Depositional processes and deposit types: Sedimentology, v. 59, p. 1937–2003, doi: 10.1111/j.1365-3091.2012.01353.x.

Teixell, A., and García-Sansegundo, J., 1995, Estructura del sector central de la Cuenca de Jaca (Pirineos meridionales): Rev. Soc. Geol. España, v. 8, no. 3, p. 215–228.

Tinterri, R., 2011, Combined flow sedimentary structures and the genetic link between sigmoidal- and hummocky-cross stratification: GeoActa, v. 10, p. 1–43, doi: -.

Tinterri, R., and Muzzi Magalhaes, P., 2011, Synsedimentary structural control on foredeep turbidites: An example from Miocene Marnoso-arenacea Formation, Northern Apennines, Italy: Marine and Petroleum Geology, v. 28, no. 3, p. 629–657, doi: https://doi.org/10.1016/j.marpetgeo.2010.07.007.

Tinterri, R., and Tagliaferri, A., 2015, The syntectonic evolution of foredeep turbidites related to basin segmentation: Facies response to the increase in tectonic confinement (Marnoso-arenacea Formation, Miocene, Northern Apennines, Italy): Marine and Petroleum Geology, v. 67, p. 81–110, doi: 10.1016/j.marpetgeo.2015.04.006.

Tinterri, R., Drago, M., Consonni, A., Davoli, G., and Mutti, E., 2003, Modelling subaqueous bipartite sediment gravity flows on the basis of outcrop constraints: First results: Marine and Petroleum Geology, v. 20, no. 6-8, p. 911–933, doi: 10.1016/j.marpetgeo.2003.03.003.

Tinterri, R., Magalhaes, P.M., Tagliaferri, A., and Cunha, R.S., 2016, Convolute laminations and load structures in turbidites as indicators of flow reflections and decelerations against bounding slopes . Examples from the Marnoso-arenacea Formation (northern Italy) and Annot Sandstones (south eastern France): Sedimentary Geology, v. 344, p. 382–407, doi: 10.1016/j.sedgeo.2016.01.023.

Tinterri, R., Laporta, M., and Ogata, K., 2017, Asymmetrical cross-current turbidite facies tract in a structurally-confined mini-basin (Priabonian-Rupelian, Ranzano Sandstone, northern Apennines, Italy): Sedimentary Geology, v. 352, p. 63–87, doi: 10.1016/j.sedgeo.2016.12.005.

Walker, R.G., 1966, Shale Grit and Grindslow shales; transition from turbidite to shallow water sediments in the upper Carboniferous of northern England: Journal of Sedimentary Research, v. 36, no. 1, p. 90–114.

Walker, R.G., 1967, Turbidite sedimentary structures and their relationship to proximal and distal depositional environments: Journal of Sedimentary Petrology, v. 37, no. 1, p. 25–43, doi: 10.1306/74D71645-2B21-11D7-8648000102C1865D.

Walker, R.G., 1978, Deep-Water Sandstone Facies and Ancient Submarine Fans: Models for Exploration for Stratigraphic Traps: AAPG Bulletin, v. 62, no. 6, p. 932–966, doi: 10.1306/C1EA4F77-16C9-11D7-8645000102C1865D.

Wynn, R.B., Weaver, P.P.E., Masson, D.G., and Stow, D.A. V, 2002, Turbidite depositional architecture across three interconnected deep-water basins on the north-west African margin: Sedimentology, v. 49, p. 669–695, doi: 10.1046/j.1365-3091.2002.00471.x.

Figure 1: A) Location of the field area in Spain; B) Simplified geological map of the Hecho Group (adapted from Remacha et al., 2003); C) Paleogeographic map of the Pyrenean Foreland Basin during the Early Lutetian (modified from Dreyer et al., 1999).

Figure 2: Stratigraphic column of the Pyrenean foreland basin fill. Nomenclature is given for the stratigraphy of the Jaca Basin (adapted from: Remacha et al., 2003; Caja et al., 2010). Several correlation schemes for the Jaca turbidite systems with those of the Aínsa Basin have been proposed (e.g. Mutti, 1985; Das Gupta and Pickering, 2008; Caja et al., 2010; Clark et al., 2017).

Figure 3: Satellite imagery of the field area showing proximal (B), distal (C) and medial (Acín; see A) localities. Transects W, X, Y and Z are illustrated in Figs. 9, 12, and 13.

Figure 4: Bed-scale facies deposited from turbidity currents, typically, but not exclusivey identified in proximal and medial localities (Fig. 3). A) Thin-bedded sandstone with planar lamination at the base and ripple-cross lamination towards the top. Identified basin-wide; B) Stepped planar-laminations observed at the most proximal location, Fanlo 2; C) Planar-laminated fine-grained sandstone; D) Structureless medium-grained sandstone with mudstone-clasts; E) Coarse-grained lag on the upper-surface of a scour. There is a grain-size break from relatively clean upper-fine sandstone to coarse and very-coarse sandstone with abundant mm- and cm-scale mudstone clasts; F) Mudstone-draped scour observed at Fanlo 2.

Figure 5: Selected hybrid bed facies demonstrating the range of bed-types observed. A) Thin hybrid bed with a thin siltstone basal division, overlain by a sharp break to D3 which has a sharp upper surface to D6; B) Hybrid bed with lower structureless sandstone with a ripple cross-lamination top. Overlain by a poorly sorted D3 and D4 which normally-grade upwards into D5 and D6; C) Lower structureless sandstone with a sharp upper contact with argillaceous sandstone D3. There is a sharp, sheared boundary between D3 and D4. D4 is gradational into D5 and D6; D) Outsized hybrid bed (Bed 2; Fig. 10). The basal 5cm consists of a lag of very coarse-grained sandstone clasts, armoured mudstone-chips and Foraminifera. Overlying is a poorly-sorted division which fines gradationally

upwards into D5 and D6; E) Inset of (C) illustrating the sharp, sheared boundary between D3 and D4 with entrianment of clasts from D3; F) Example of D3 containing clasts of underlying D1.

Figure 6: A) Lenticular, hummock-type bedform observed at Hecho N (Fig. 3C). B) Convolute laminations observed at Acín (Fig. 3A). C) Hummock-type bedform observed at Hecho N.

Figure 7: Contact of Db-1 with substrate near the Yésero locality (Fig. 3). Local entrainment of substrate appears to occur through a stepped delamination process similar to that described in turbidites and hybrid beds (Butler and Tavarnelli, 2006; Eggenhuisen et al., 2011; Fonnesu et al., 2016).

Figure 8: A, B) Overview of the proximal stratigraphy in cliffs adjacent to the Fanlo 1 locality (Barranco El Chate Cliffs; Fig. 3). Several of the described sandstone lobes are observed (numbered), along with 3 marker beds (Db 1, Db 2 and MT-4); C) The transition of Lobe 6 from bypass-dominated features to deposition-dominated features is observed in the cliffs, potentially forming a sand-detached lobe (at least in two-dimensions); D) Line drawing of (C).

Figure 9: A) Paleocurrent data collected within the field area. Proximal data are collected from flutes, grooves and ripple crests which are consistent in trend and are grouped together (n=57). Medial and distal localities are segregated by paleocurrent indicator. Data show that flute and groove marks (n=103) diverge from ripple cross-laminations (n=6) directions in medial and distal locations. Flutes and grooves formed at the bed bases, whereas ripple cross-lamination formed on bed tops, suggesting the initial and later stages of the flows had divergent paleoflow directions. Refer to Figure 1 for key to stratigraphy, map modfied from Remacha et al., (2003); B) Example of a single bed with divergent paleocurrent indicators at the bed base and bed top. This suggests that the initial flow was to the northwest, while a later, deflected flow-component was to the north.

Figure 10: Down depositional-dip oriented correlation panel from proximal to distal (right to left), note changes in horizontal scale. Log locations are shown in Fig. 3. Logs are tied to the basin-wide MT-4 marker bed. There is an overall fining, and thinning at both bed- and lobe-scale between Fanlo 2 and Yésero 2. Lobes Ac1-4 at Acín are thicker bedded and coarser than at Yésero and Linás de

Broto, suggesting the flows which deposited these lobes bypassed the proximal area of the system. Beds in distal localities (west of Acín) do not form well-developed lobes. Lobe 4 is not observed in the panel as it pinches out to the north of Fanlo 1.

Figure 11: Graphs illustrating the spatial variability of hybrid bed abundance and proportional thickness: A) Down-dip from proximal localities to distal localities; B) across strike in distal localities.

Figure 12: Stratigraphic interpretations of proximal lobes and geometry of Lobe 6. Lobes exhibit lateral facies changes on a kilometer-scale. Lobe 6 is not observed at Fanlo 1, whereas it is observed to the north and south at Fanlo Track and El Chate Cliffs (Fig. 8) respectively. The stratigraphy can be walked 1.5 km to the west to Barranco El Chate where Lobe 6 is 9 m-thick.

Figure 13: Across strike architectural panels at the distal locations of Ansó (A) and Hecho (B; Fig. 3): A) The Ansó strike panel is tied to the mudstone cap of MT-4. Tentative individual bed correlations are indicated by dotted lines. B) The Hecho panel is tied to the base of MT-4 as the top of the unit is difficult to access. Individual bed correlations are challenging to make due to the disparity in facies between the two outcrops over relatively short distances.

Figure 14: Model to explain the facies, structures and paleocurrents observed: A) Deflected flows with differing rheological properties rework and/or shear previous deposits. The initial deflected, turbulent, flow reworks the bed-top (2) of the non-deflected flow deposit (1) and is followed by deflected flows which entrained slope substrate, becoming cohesive (3). Later parts of the flow are more dilute and carbonate-rich (4); B) Schematic reconstruction of the depostion of a characteristic bed by a flow transitional between turbulent (TF) and laminar (LF) flow regimes.

Figure 15: A) Schematic interpretation of the Jaca Basin paleogeography during deposition of the Upper Broto turbidite system; B) Proximally, lobes stacked compensationally, and did not develop hybrid beds. The solid colour box is based on data presented in Fig. 12; C) Distally, flows were able to interact with the southern carbonate margin, which deflected flow-components to the north. These deflected flows entrained carbonate-rich muddy slope material, increasing flow cohesion; these

flows then deposited the hybrid bed D3 and D4 overlying the primary deposits not affected by the slope.

Figure 16: Schematic illustration of how deflected cohesive flows can influence depositional topography. The relative across-strike orientation of the primary (orange) and deflected (purple) flows develop perpendicular to each other, creating subtle topography which could influence the architecture of subsequent flows.

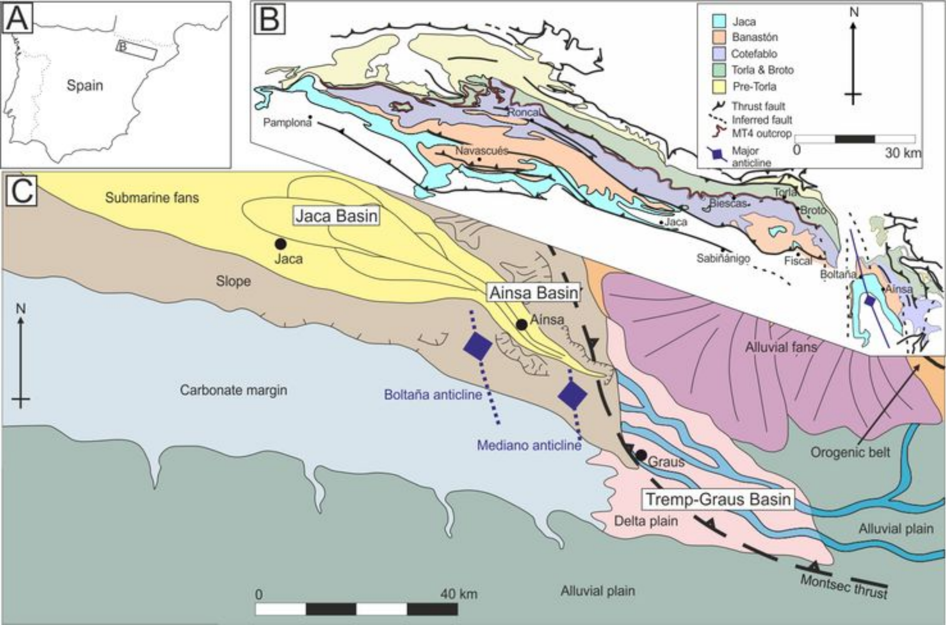
A
B
Spain
Jaca
Banastón
Cotefablo
Torla & Broto
Pre-Torla
Thrust fault
Inferred fault
MT4 outcrop
Major anticline
N
0
30 km
Pamplona
Roncal
Navascués
Torla
Biescas
Broto
Jaca
Sabiñánigo
Fiscal
Boltaña
Aínsa
C
Submarine fans
Jaca Basin
Jaca
Slope
Ainsa Basin
Aínsa
Carbonate margin
Boltaña anticline
Mediano anticline
Graus
Tremp-Graus Basin
Delta plain
Alluvial fans
Orogenic belt
Alluvial plain
Montsec thrust
Alluvial plain
N
0
40 km

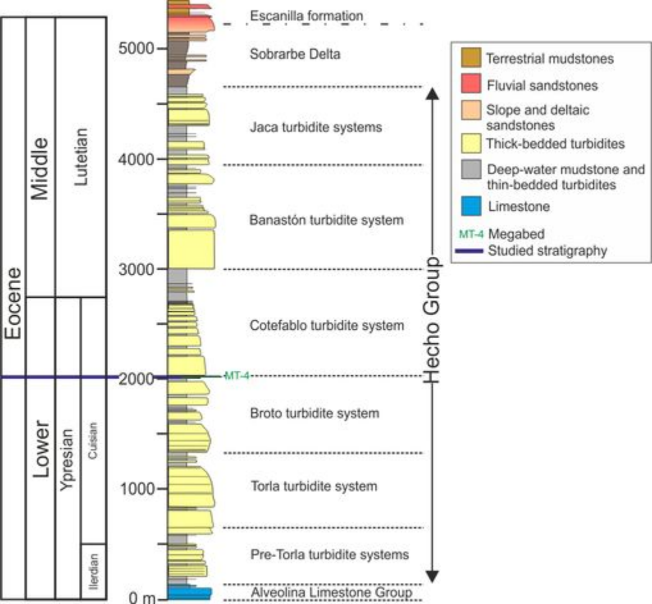

Eocene
Middle
Lutetian
Lower
Ypresian
Cuisian
Ilerdian
5000
4000
3000
2000
1000
0 m
Escanilla formation
Sobrarbe Delta
Jaca turbidite systems
Banastón turbidite system
Cotefablo turbidite system
MT-4
Broto turbidite system
Torla turbidite system
Pre-Torla turbidite systems
Alveolina Limestone Group
Hecho Group
Terrestrial mudstones
Fluvial sandstones
Slope and deltaic sandstones
Thick-bedded turbidites
Deep-water mudstone and thin-bedded turbidites
Limestone
MT-4 Megabed
Studied stratigraphy

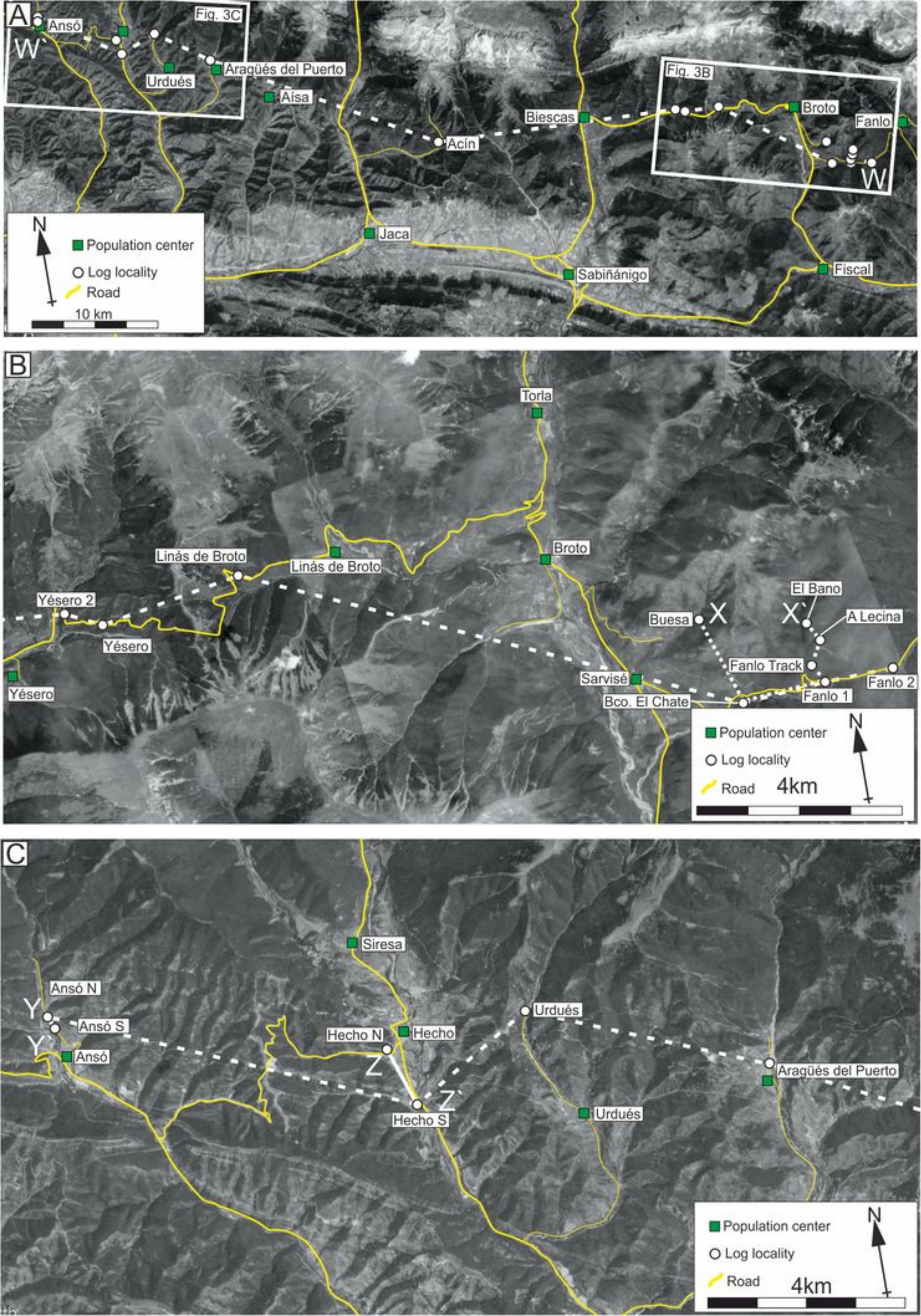
A
Ansó
W`
Fig. 3C
Urdués
Aragüés del Puerto
Aisa
Acín
Biescas
Fig. 3B
Broto
Fanlo
W
Jaca
Sabiñánigo
Fiscal
N
Population center
Log locality
Road
10 km
B
Torla
Linás de Broto
Linás de Broto
Broto
Yésero 2
Yésero
Yésero
Buesa
X
El Bano
X`
A Lecina
Fanlo Track
Fanlo 1
Fanlo 2
Sarvisé
Bco. El Chate
Population center
Log locality
Road
4km
N
C
Siresa
Ansó N
Y
Ansó S
Y`
Ansó
Hecho N
Hecho
Z
Z`
Hecho S
Urdués
Urdués
Aragüés del Puerto
Population center
Log locality
Road
4km
N

Table 1: Summary of lithofacies observed in the study area.

Facies	Lithology	Sedimentology	Thickness (m)	Interpretation
Structureless sandstone	Very fine- to medium-grained sandstone, rare coarse-grained sandstone. Siltstone caps are infrequently present in distal localities but are not present in proximal localities.	Typically structureless and frequently normally-graded or coarse-tail graded. Occasional mudstone chips occur, typically in fine- to coarse-grained sandstone beds. *Nummulites* are infrequently observed.	0.05 – 0.5	Rapid aggradation from a high-concentration flow (Lowe, 1982; Mutti, 1992; Kneller and Branney, 1995).
Stepped-planar-laminated sandstone	Medium- to coarse-grained sandstone.	Laminated sandstone, laminae are 5 – 15 mm thick, parallel to sub-parallel and typically coarser grained than surrounding sandstone. Coarser laminae are typically inversely graded.	0.1 – 0.5	Repeated collapse of traction carpets below a high-concentration turbidity current (Talling et al., 2012; Cartigny et al., 2013).
Planar-laminated sandstone	Very fine- to medium-grained sandstone.	Laminated sandstone with µm – mm scale alternating coarser – finer laminae. Laminae are typically parallel, rarely sub-parallel. Common coarse-tail grading. Infrequent occurrence of plant fragments and mudstone chips aligned with laminae.	0.04 – 0.5	Layer-by-layer deposition from repeated development and collapse of near-bed traction carpets (Sumner et al., 2008) and migration of low-amplitude bed-waves (Best and Bridge, 1992; Sumner et al., 2008).
Ripple-laminated sandstone	Very fine- to fine-grained sandstone, rarely medium-grained sandstone and coarse siltstone.	Ripple-cross laminations, typically located in the upper parts of the bed. Climbing ripples locally observed. Commonly produces wavy bed tops.	0.02 – 0.1	Tractional reworking beneath a dilute, slow-moving flow (Allen, 1982; Southard, 1991).
Convolute ripple cross laminations	Very fine- to fine-grained sandstone.	Deformed, folded and overturned ripple cross lamination.	0.02 – 0.1	Liquefaction due to loading of overlying sediment (Allen, 1982), or shear stresses caused by subsequent flow (Allen, 1982; McClelland et al., 2011; Tinterri et al., 2016).
Hummock-type bedforms	Very fine- to fine-grained sandstone.	Decimeter- to meter-wavelength undulating bedforms. Typically consist of smaller-scale wavy, convolute or ripple cross-laminations.	0.02 – 0.15	Reworking of initial deposit of a bipartite flow by a bypassing flow-component (Mutti, 1992; Tinterri et

				al., 2017), or reworking of initial flow deposits by internal bores within a deflected flow (Pickering and Hiscott, 1985; Remacha et al., 2005).
Argillaceous sandstone	Poorly-sorted, claystone- and siltstone-rich sandstone.	Beds have higher mud contents in the matrix compared to relatively clean sandstone beds. Infrequently contain spheroidal or folded sandstone and mm-scale mudstone blebs. Where two argillaceous sandstones overlie each other, delamination and shearing structures are sometimes observed.	0.05 – 0.3	Transitional flow deposit (Sylvester and Lowe, 2004; Baas et al., 2009; Sumner et al., 2009; Kane and Pontén, 2012).
Poorly-sorted mudstone	Siltstone- and sandstone-rich claystone	Commonly graded into mudstone; however, infrequent non-graded, sharp-topped examples occur. Mudstone- and siltstone-clasts, and mudstone-armoured *Nummulites* are frequently present. Clasts are commonly present as sub-rounded balls or as plastically deformed layers. Infrequent disaggregated and sheared layers are observed. Where overlying argillaceous sandstone, delamination and shearing structures are sometimes observed.	0.05 – 3.2	Clast-rich, poorly-sorted, matrix supported beds are suggestive of *en-masse* deposition from laminar flows (e.g. Nardin et al., 1979; Iverson, 1997; Sohn, 2000). Beds which exhibit grading are likely to have retained some level of turbulence within the flow; and are therefore interpreted to have deposited from a transitional-flow regime (Baas et al., 2009; Sumner et al., 2012; Baas et al., 2013).
Carbonate-rich siltstone	Carbonate-rich siltstone. Rare carbonate-rich mudstone.	Distinctive off-white colour. Exhibits a gradational base where overlying graded mudstones, but is often sharp where overlying argillaceous sandstone. Generally homogenous texture.	0.02 – 0.3	Fine-grained carbonate hydraulically fractionated from siliciclastics, deposited from dilute remnants of the flow (Remacha and Fernández, 2003).
Matrix-supported chaotic deposits	Poorly-sorted, clast-rich matrix consisting of sandstone, siltstone and mudstone.	Clasts include: cm – m scale sandstone balls, m – 10s m scale sandstone rafts, dm – m scale mudstone rafts. Sandstone rafts are frequently found at the top of the beds.	0.2 – 25	“Freezing” of a flow with yield strength, i.e. a debris flow (e.g. Iverson et al., 2010).
Mudstone	Silt-rich mudstone	Massive- to weakly-laminated.	0.01 – 2.5	Background sedimentation or

deposition from a dilute flow.

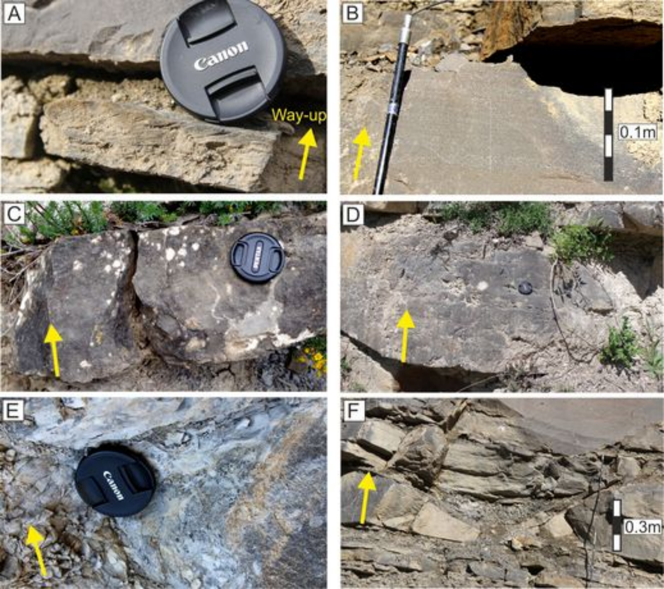
A
Canon
Way-up
B
0.1m
C
D
E
Canon
F
0.3m

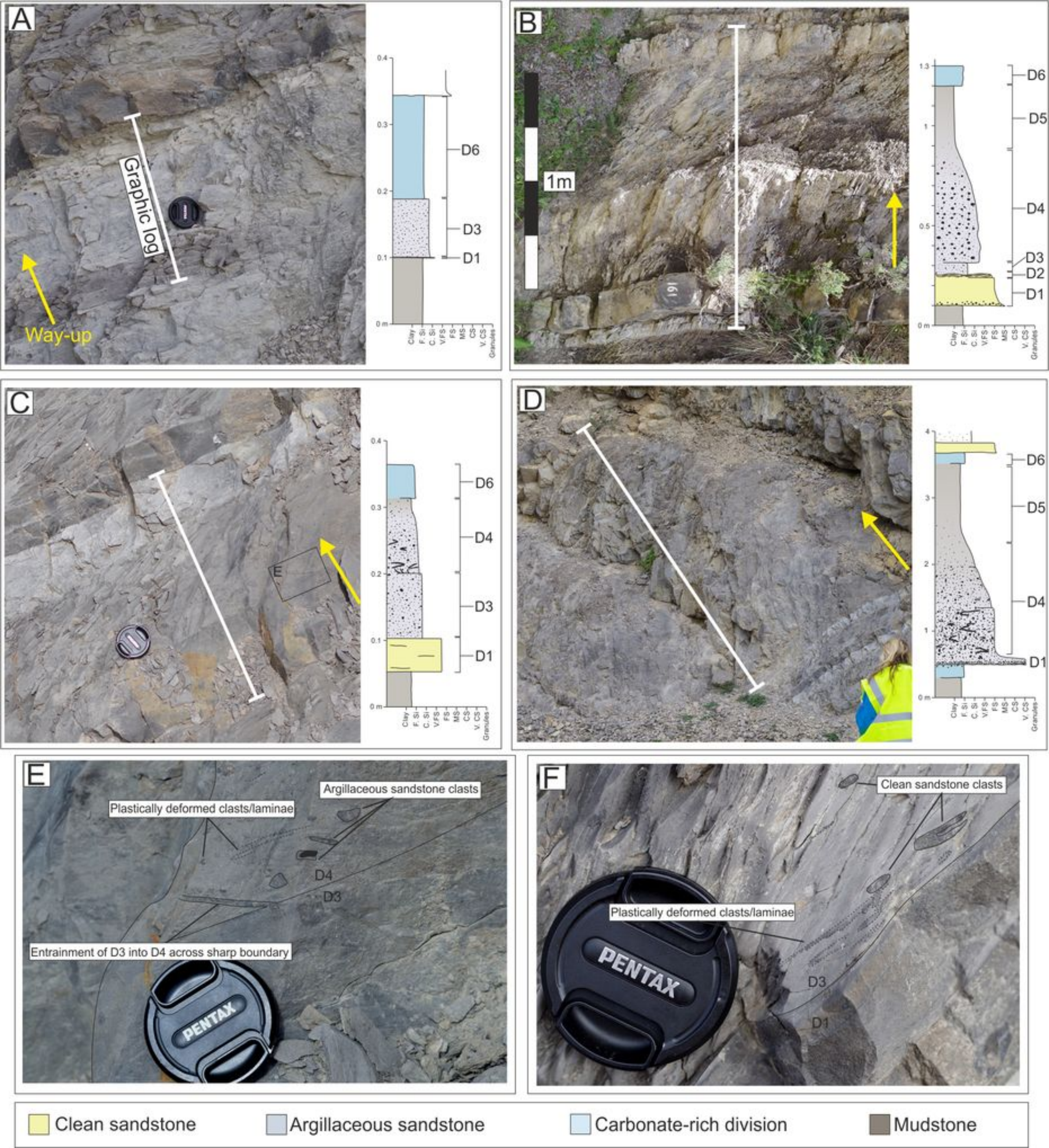
A
Graphic log
Way-up
0.4
0.3
0.2
0.1
0 m
D6
D3
D1
Clay
F. Si
C. Si
VFS
FS
MS
CS
V. CS
Granules
B
1m
1.3
1
0.5
0 m
D6
D5
D4
D3
D2
D1
C
E
D6
D4
D3
D1
D
4
3
2
1
0 m
D6
D5
D4
D1
E
Argillaceous sandstone clasts
Plastically deformed clasts/laminae
D4
D3
Entrainment of D3 into D4 across sharp boundary
PENTAX
F
Clean sandstone clasts
Plastically deformed clasts/laminae
D3
D1
PENTAX
Clean sandstone
Argillaceous sandstone
Carbonate-rich division
Mudstone

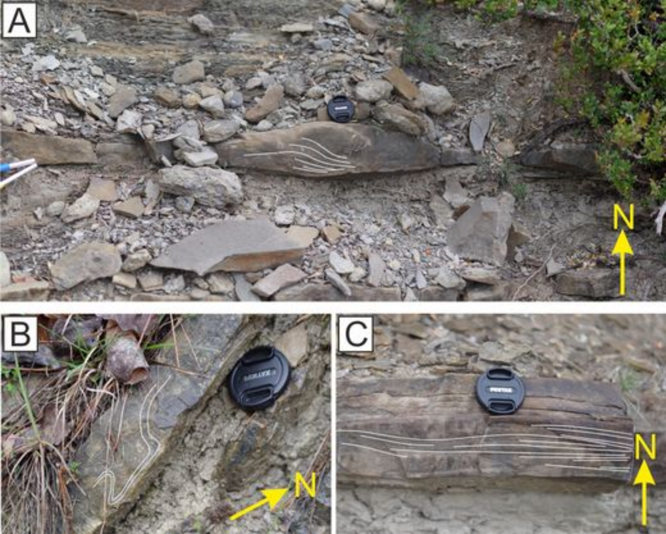
A
N
B
N
C
N

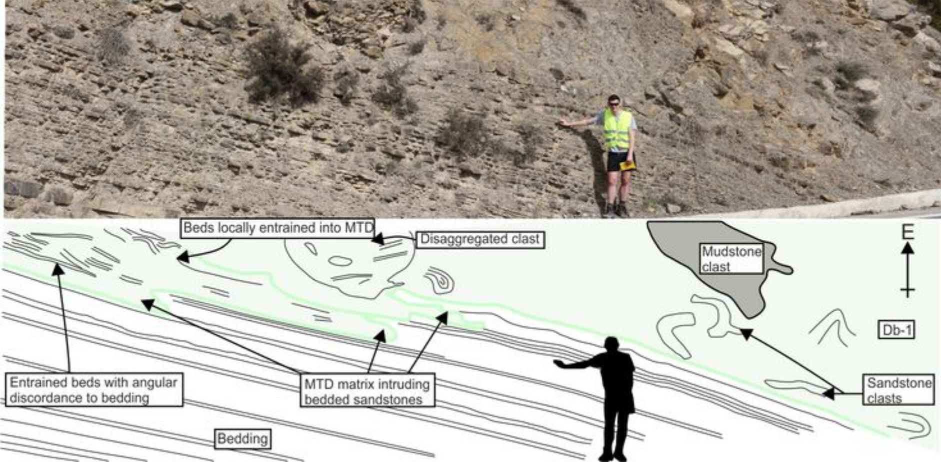
Beds locally entrained into MTD
Disaggregated clast
Mudstone clast
E
Db-1
Entrained beds with angular discordance to bedding
MTD matrix intruding bedded sandstones
Sandstone clasts
Bedding

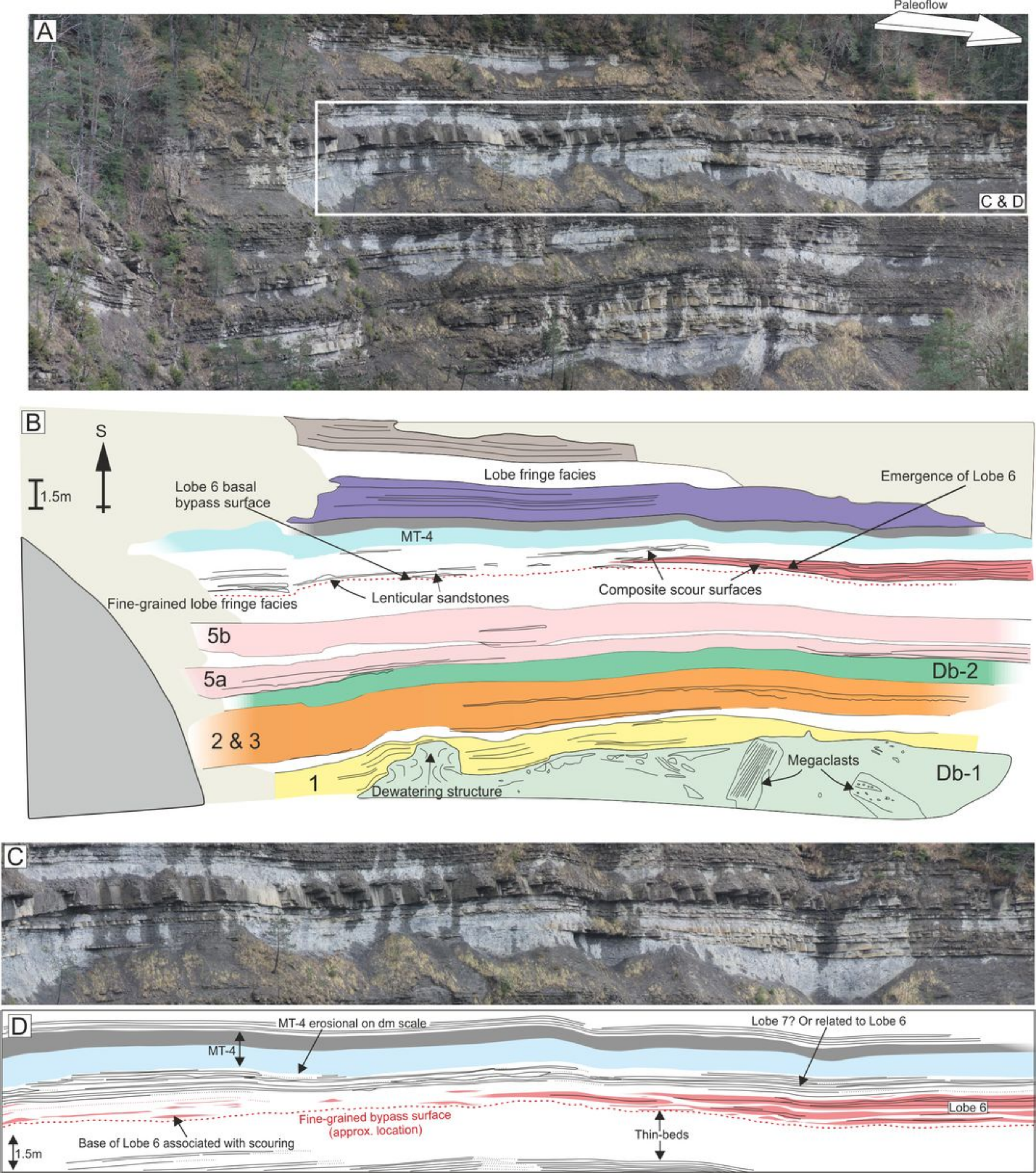

A
Paleoflow
C & D
B
S
1.5m
Lobe fringe facies
Emergence of Lobe 6
Lobe 6 basal
bypass surface
MT-4
Composite scour surfaces
Lenticular sandstones
Fine-grained lobe fringe facies
5b
5a
Db-2
2 & 3
Megaclasts
1
Dewatering structure
Db-1
C
D
MT-4 erosional on dm scale
Lobe 7? Or related to Lobe 6
MT-4
Lobe 6
Fine-grained bypass surface
(approx. location)
Base of Lobe 6 associated with scouring
Thin-beds
1.5m

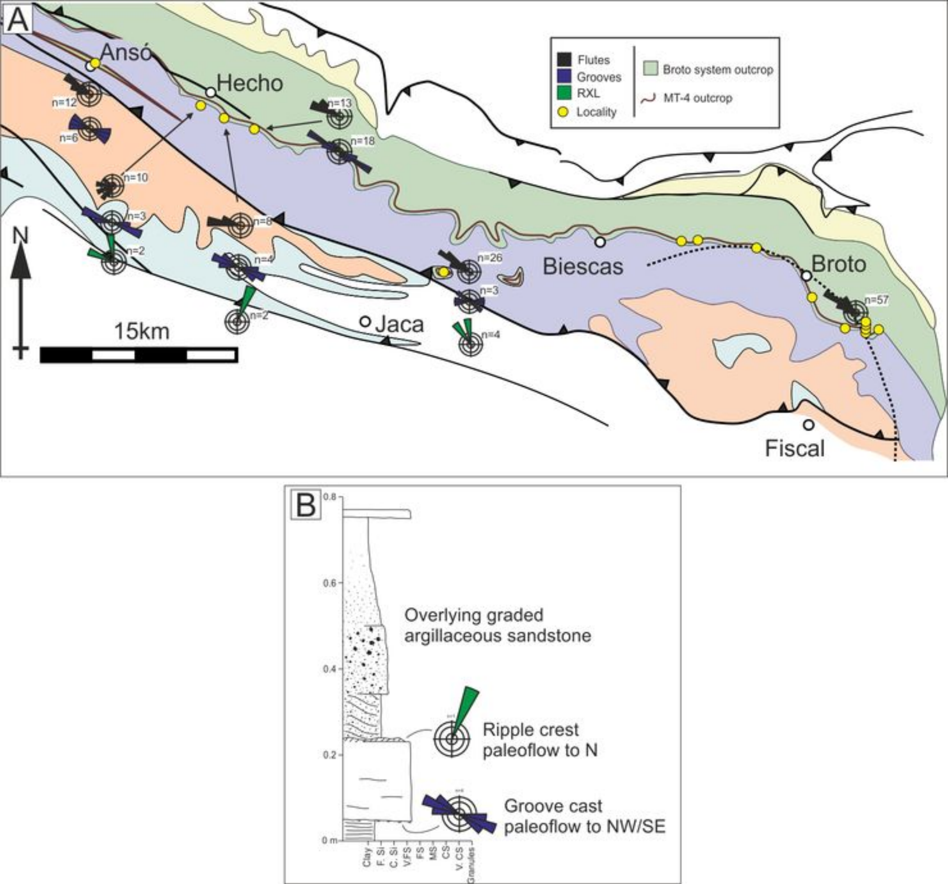
A
Ansó
Hecho
Biescas
Broto
Jaca
Fiscal
15km
N
Flutes
Grooves
RXL
Locality
Broto system outcrop
MT-4 outcrop
n=12
n=6
n=10
n=3
n=2
n=8
n=4
n=2
n=13
n=18
n=26
n=3
n=4
n=57
B
Overlying graded argillaceous sandstone
Ripple crest paleoflow to N
Groove cast paleoflow to NW/SE
0.8
0.6
0.4
0.2
0 m
Clay
F. Si
C. Si
VFS
FS
MS
CS
V. CS
Granules

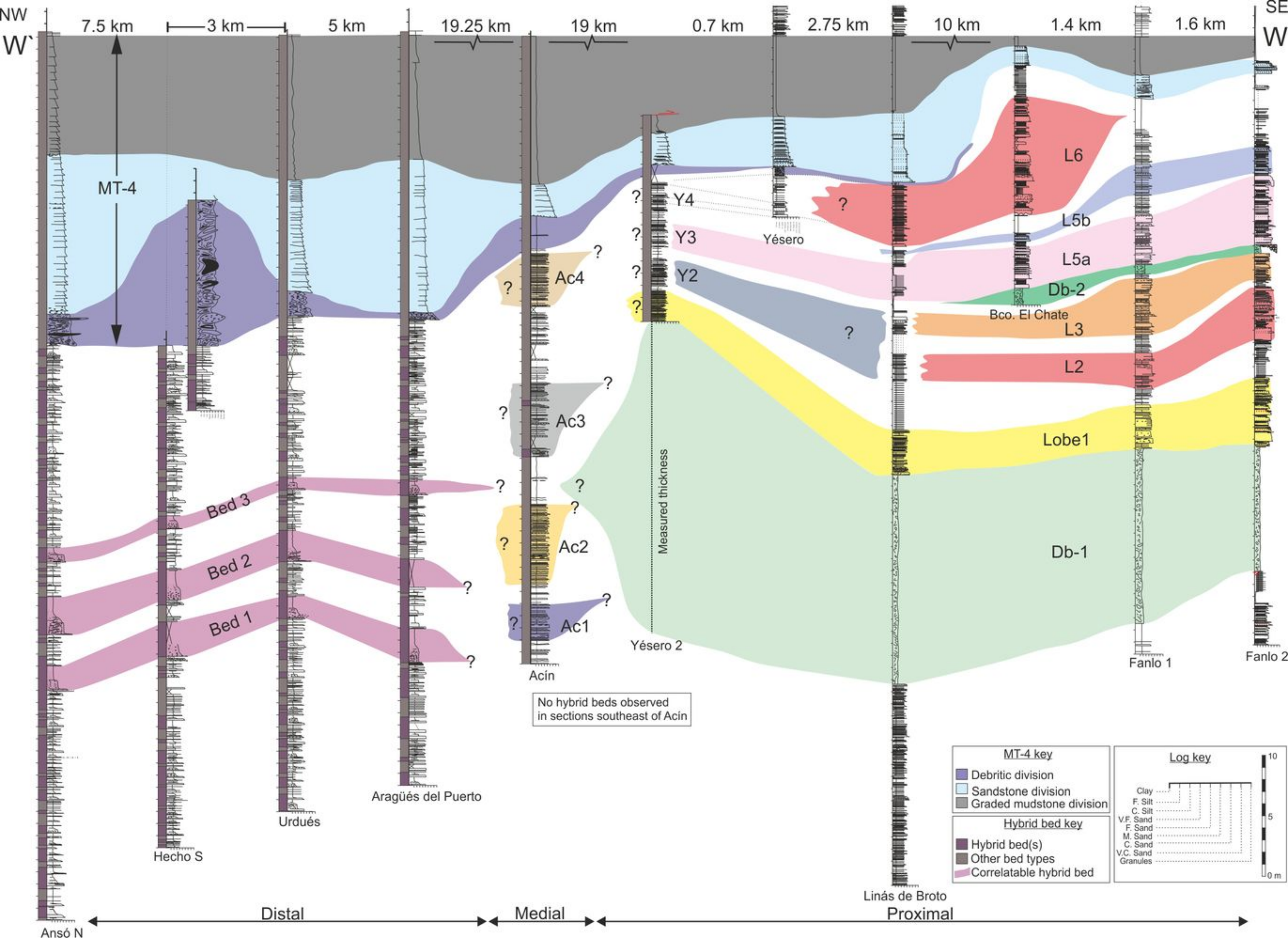
NW
W`
SE
W
7.5 km
3 km
5 km
19.25 km
19 km
0.7 km
2.75 km
10 km
1.4 km
1.6 km
MT-4
Bed 3
Bed 2
Bed 1
Ac4
Ac3
Ac2
Ac1
Y4
Y3
Y2
Measured thickness
Yésero
Yésero 2
L6
L5b
L5a
Db-2
Bco. El Chate
L3
L2
Lobe1
Db-1
Ansó N
Hecho S
Urdués
Aragüés del Puerto
Acín
Linás de Broto
Fanlo 1
Fanlo 2
No hybrid beds observed in sections southeast of Acín
MT-4 key
Debritic division
Sandstone division
Graded mudstone division
Hybrid bed key
Hybrid bed(s)
Other bed types
Correlatable hybrid bed
Log key
Clay
F. Silt
C. Silt
V.F. Sand
F. Sand
M. Sand
C. Sand
V.C. Sand
Granules
10
5
0 m
Distal
Medial
Proximal

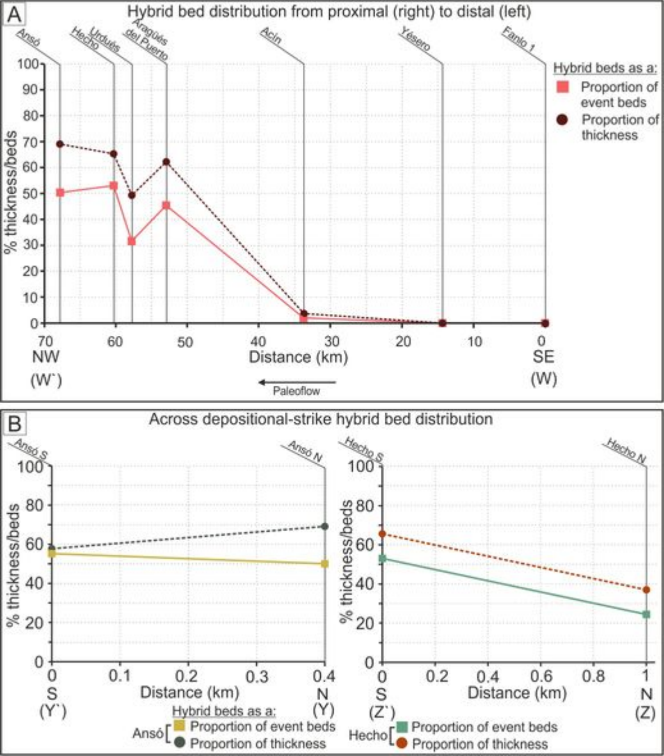
A
Hybrid bed distribution from proximal (right) to distal (left)
Ansó
Hecho
Urdués
Aragüés del Puerto
Acín
Yésero
Fanlo 1
% thickness/beds
Hybrid beds as a:
Proportion of event beds
Proportion of thickness
NW (W`)
Distance (km)
SE (W)
Paleoflow
B
Across depositional-strike hybrid bed distribution
Ansó S
Ansó N
Hecho S
Hecho N
% thickness/beds
S (Y`)
Distance (km)
N (Y)
S (Z`)
N (Z)
Hybrid beds as a:
Ansó
Proportion of event beds
Proportion of thickness
Hecho
Proportion of event beds
Proportion of thickness

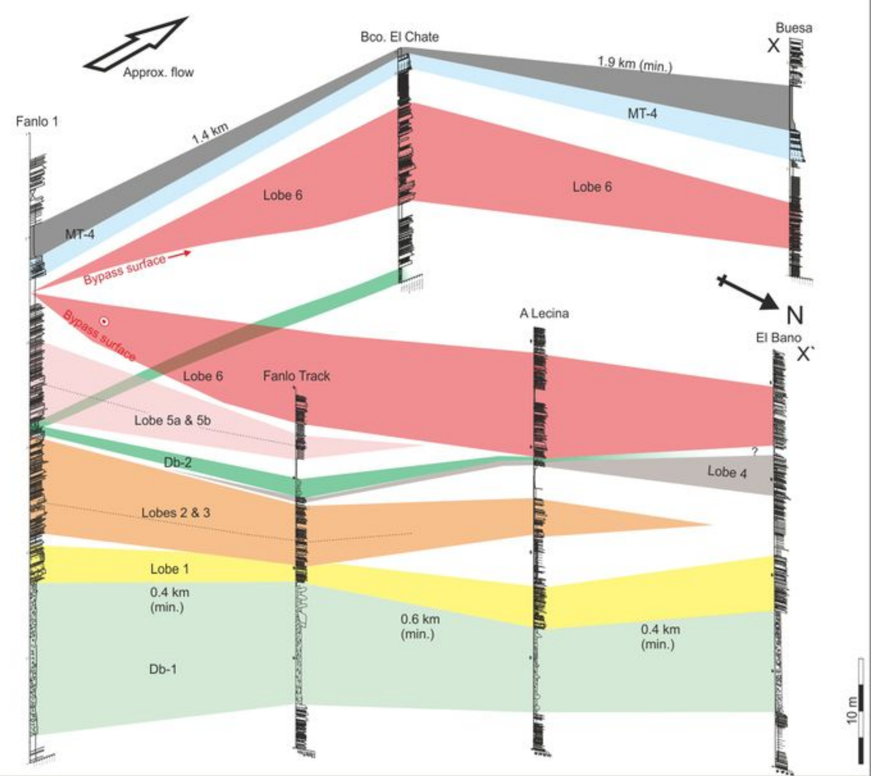

Approx. flow
Bco. El Chate
Buesa
X
1.9 km (min.)
Fanlo 1
1.4 km
MT-4
Lobe 6
Lobe 6
MT-4
Bypass surface
Bypass surface
N
A Lecina
El Bano
X`
Lobe 6
Fanlo Track
Lobe 5a & 5b
Db-2
?
Lobe 4
Lobes 2 & 3
Lobe 1
0.4 km
(min.)
0.6 km
(min.)
0.4 km
(min.)
Db-1
10 m

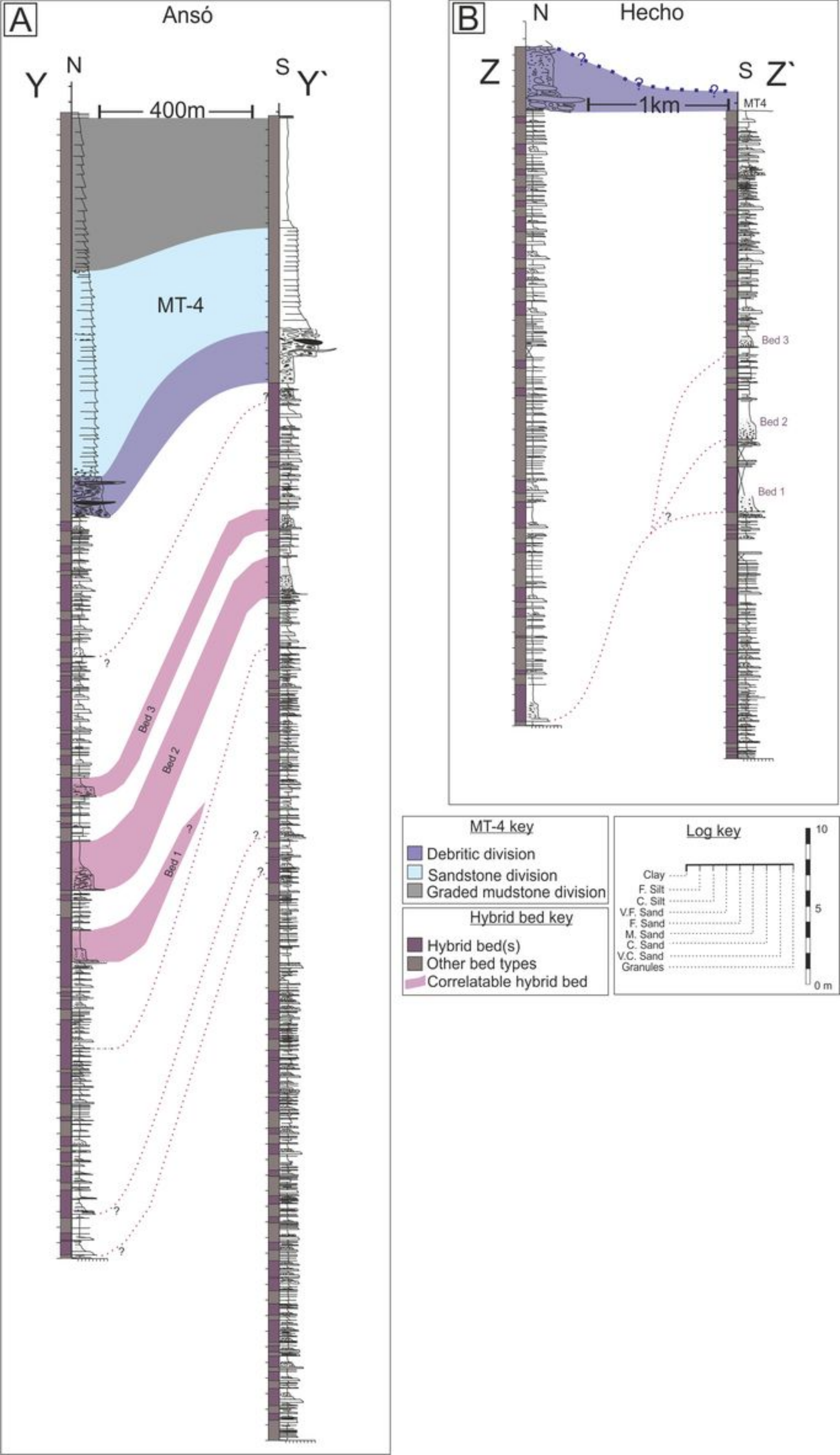
A
Ansó
Y
N
S
Y`
400m
MT-4
Bed 3
Bed 2
Bed 1
?
B
Hecho
Z
N
S
Z`
1km
MT4
Bed 3
Bed 2
Bed 1
MT-4 key
Debritic division
Sandstone division
Graded mudstone division
Hybrid bed key
Hybrid bed(s)
Other bed types
Correlatable hybrid bed
Log key
Clay
F. Silt
C. Silt
V.F. Sand
F. Sand
M. Sand
C. Sand
V.C. Sand
Granules
10
5
0 m

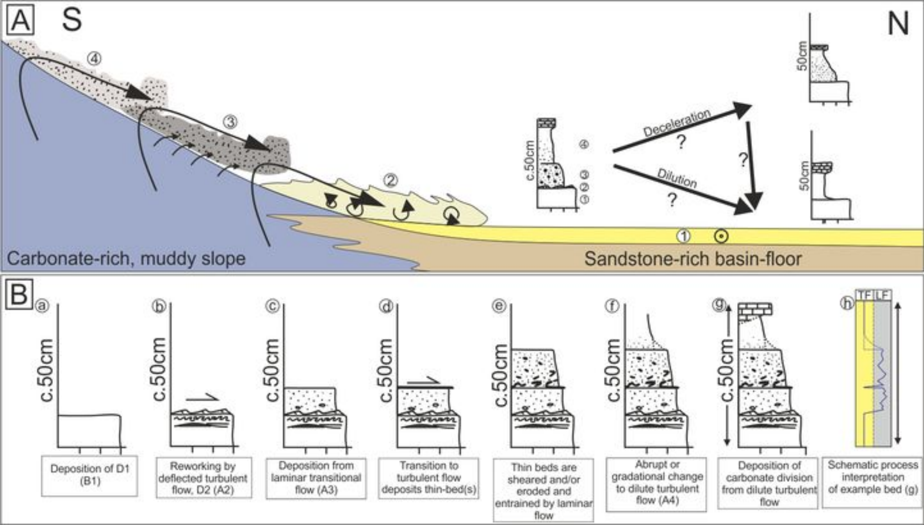

A
S
N
④
③
②
①
c.50cm
50cm
50cm
Deceleration
Dilution
?
?
?
Carbonate-rich, muddy slope
Sandstone-rich basin-floor
B
a
b
c
d
e
f
g
h
c.50cm
c.50cm
c.50cm
c.50cm
c.50cm
c.50cm
c.50cm
TF
LF
Deposition of D1 (B1)
Reworking by deflected turbulent flow, D2 (A2)
Deposition from laminar transitional flow (A3)
Transition to turbulent flow deposits thin-bed(s)
Thin beds are sheared and/or eroded and entrained by laminar flow
Abrupt or gradational change to dilute turbulent flow (A4)
Deposition of carbonate division from dilute turbulent flow
Schematic process interpretation of example bed (g)

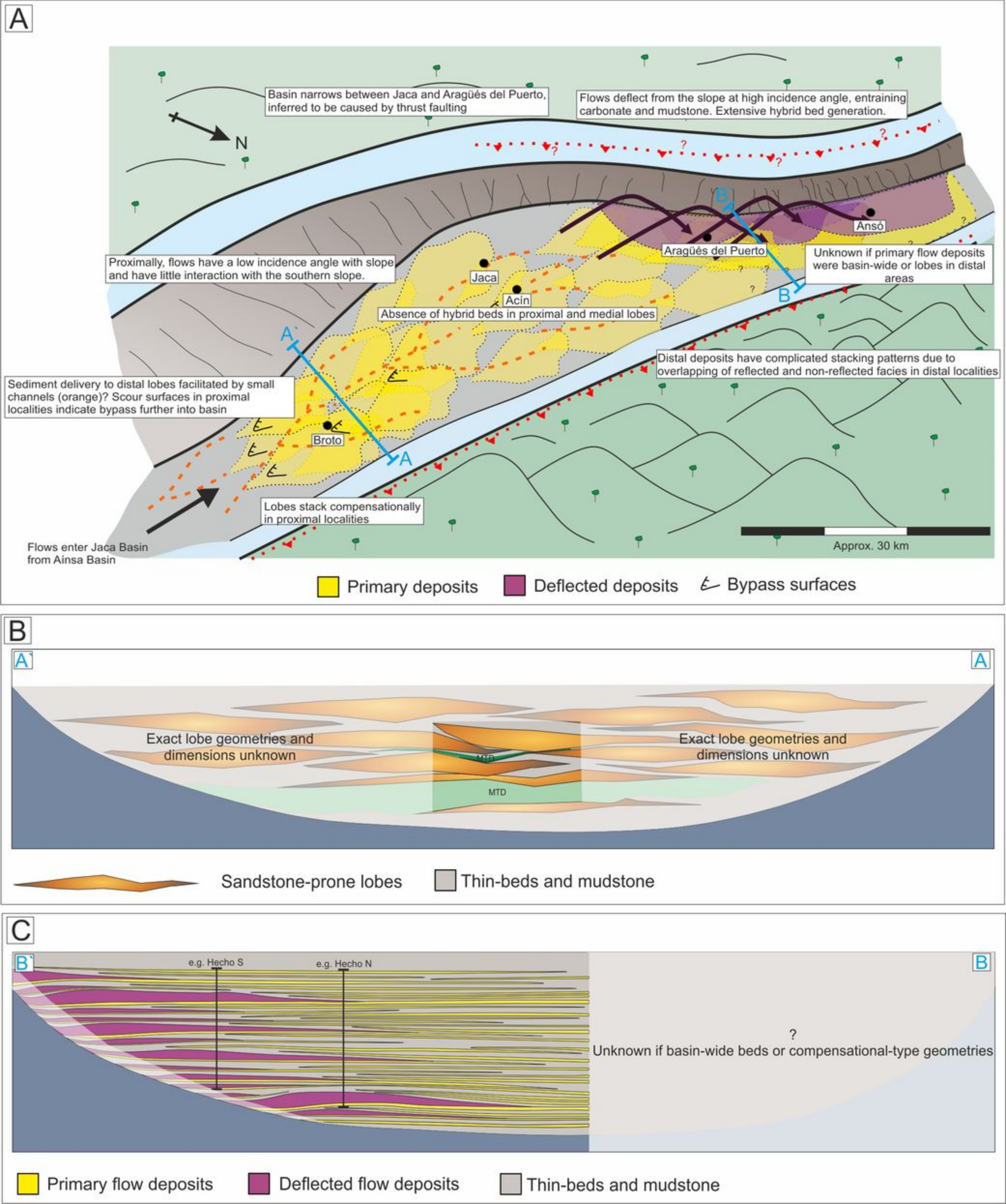
A
Basin narrows between Jaca and Aragüés del Puerto, inferred to be caused by thrust faulting
Flows deflect from the slope at high incidence angle, entraining carbonate and mudstone. Extensive hybrid bed generation.
N
Ansó
Aragüés del Puerto
Unknown if primary flow deposits were basin-wide or lobes in distal areas
Proximally, flows have a low incidence angle with slope and have little interaction with the southern slope.
Jaca
Acín
Absence of hybrid beds in proximal and medial lobes
Distal deposits have complicated stacking patterns due to overlapping of reflected and non-reflected facies in distal localities
Sediment delivery to distal lobes facilitated by small channels (orange)? Scour surfaces in proximal localities indicate bypass further into basin
Broto
Lobes stack compensationally in proximal localities
Flows enter Jaca Basin from Aínsa Basin
Approx. 30 km
Primary deposits
Deflected deposits
Bypass surfaces
B
A`
A
Exact lobe geometries and dimensions unknown
Exact lobe geometries and dimensions unknown
MTD
MTD
Sandstone-prone lobes
Thin-beds and mudstone
C
B`
B
e.g. Hecho S
e.g. Hecho N
?
Unknown if basin-wide beds or compensational-type geometries
Primary flow deposits
Deflected flow deposits
Thin-beds and mudstone

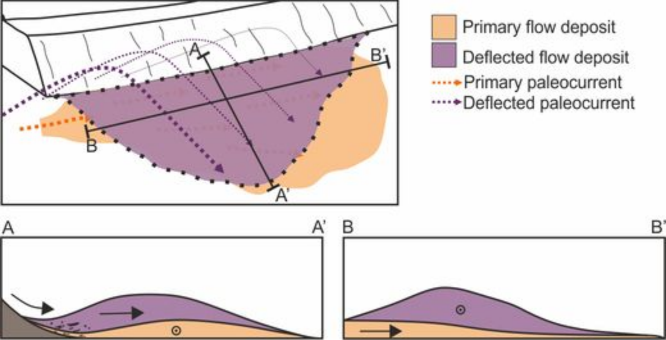

Primary flow deposit
Deflected flow deposit
Primary paleocurrent
Deflected paleocurrent
A
A'
B
B'
A
A'
B
B'